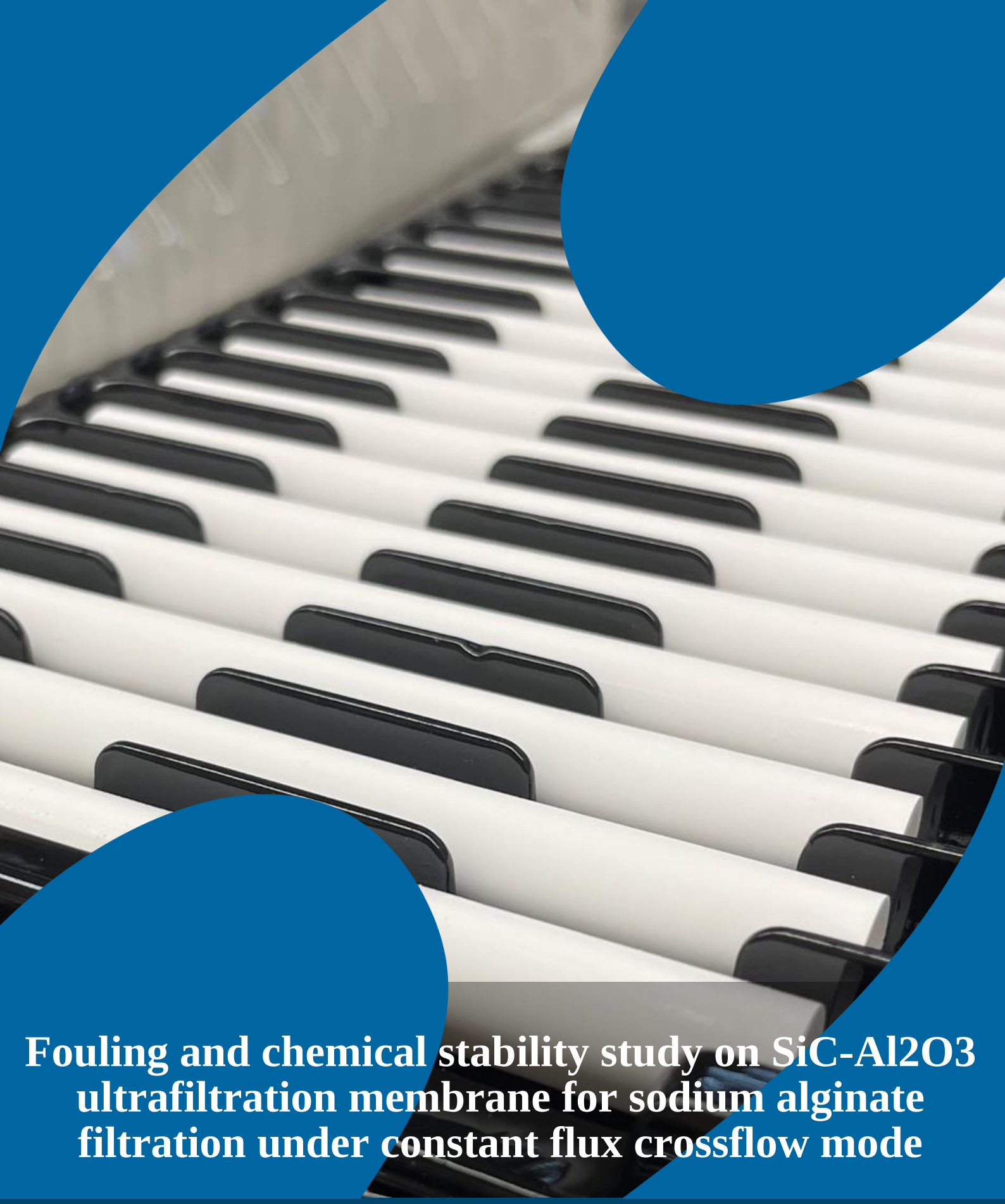

Fouling and chemical stability study on SiC-Al2O3 ultrafiltration membrane for sodium alginate filtration under constant flux crossflow mode

MSc Thesis - Luqianxue Zhang

TU Delft

Delft University of Technology

Sanitary Engineering

Fouling and chemical stability study on SiC-Al_2O_3 ultrafiltration membrane for sodium alginate filtration under constant flux crossflow mode

By

Luqianxue Zhang

In partial fulfilment of the requirements for the degree of

Master of Science

In Applied Earth Science

Publicly defended on September 29th 2022

Thesis committee: Dr. ir. Sebastian G. J. Heijman (Chair) TU Delft

Prof. dr. ir. L.C. Rietveld TU Delft

Prof. dr. ir. Jules van Lier TU Delft

Asif Jan TU Delft

Department of Sanitary Engineering

Faculty of Civil Engineering and Geoscience

Delft University of Technology

TU Delft

Abstract

Trials of surface modifications using low pressure chemical vapor deposition (LPCVD) has successfully decreased the high temperature needed for the fabrication of SiC membrane from 2000°C to below 900 °C. With this great success on the reduction of the energy consumption, however, further studies on the chemical stability and the fouling features of this kind of membrane were necessary. In this research, experiments were done on the SiC-Al_2O_3 UF membrane fabricated by LPCVD to study its chemical stability in a NaClO solution and its fouling features when filtrating sodium alginate and surface water under constant flux cross-flow mode. The backwash efficiency and the fouling resistance were analysed as well to further elucidate the fouling composition.

According to the results, the SiC-Al_2O_3 membrane coated under higher temperature (860°C) remained stable in the NaClO solution for 200 h, (1% for 100 h and then 5% for 100 h) while the membrane coated under lower temperature (750°C) showed a water permeability increase during chlorine treatment, indicating the dissolution of the SiC layer. The high temperature coated membrane (860°C) had a better antifouling ability than low temperature coated membrane (750°C) and the pristine membrane especially when filtrating the pure sodium alginate (SA) solution without Ca^{2+} under normal flux (170 LMH) or the surface water under lower flux (65 LMH). Cake filtration was observed in the fouling curves when the critical flux was not exceeded. The addition of Ca^{2+} into the pure SA solution resulted in the decrease of electrical repulsion and the increase of bridging between foulants and membrane surface. These led to the severe fouling of the high temperature coated membrane. The low temperature coated membrane had better antifouling ability than high temperature coated membrane and the pristine membrane when 2 mmol/L of Ca^{2+} was added. However, the backwash (backwash flux of around 340 LMH for normal flux condition and around 195 LMH for lower flux condition) was not efficient for all the membranes and should be improved in the future experiments.

Acknowledgement

With this work done, it comes to the end of my 25 month's master academic life in the Netherlands, and also a pause of my 3.5 years of abroad living. I still recalled why I chose this major before I started my bachelor project and sticked to it before I applied for a master project: I love nature and I want to help eliminate the damage human activities cause to the environment. After one year of intensive course, water treatment, especially membrane filtration became my academic study target and the optimal choice for the future career. Then 10 months of master thesis project began. Even though with everything scheduled and later done step by step, problems, confusion and depression still occurred. Luckily I got help from my supervisors, friends and families who were always willing to listen to my trouble and offer some suggestions.

First I'd like to offer my greatest gratitude to Bas Heijman and Asif Jan, who provided great support from the beginning of my thesis project to the end. I organized weekly meeting with Bas to report the progress and raise questions. Bas was always willing to offer his professional advice, clarify knowledge I had doubt with and suggest a further study direction. Asif dropped by the lab almost every working day to check out my progress and solve problems I met. With great sense of humour, he cheered me up during my experiment days. He introduced me to his PhD fellows as well, so I got the chance to make some new friends to talk to and had lunch with in the water lab. What's more, Asif also offered me suggestions of career choices and academic place. I also want to thank my committee members Luuk Rietveld and Jules van Lier who kindly started casual chat before my kick-off meeting and mid-term meeting to relief most of my nervousness. They also provided me with some constructive suggestions during the meeting to improve my thesis framework and details. Lab technicians Armand and Jasper are also nice and helpful when I needed to fix something or purchase something. My thankfulness also goes to my friends: Anita Tang, Yidan Xu, Hong Ting Au, Qinying Zha, Sovannmonica Ek and Guilherme. We did experiments together, studied together, had lunch together, hanged out together and shared daily life with each other. They brought in joy and energy to my tiring and busy days. Last but not least, I want to show my deepest longing and love for my family, who supported all the decisions I made during my life abroad and kept worrying about me when I was not by their side.

Luqianxue Zhang, Delft, September 2022

Content

1 Introduction 1
1.1 Research context 1
1.2 Research objectives and questions 3
1.3 Research approaches 4
2 Theoretical background 5
2.1 Ceramic membrane filtration 5
2.1.1 Membrane structures and configurations 6
2.1.2 Tubular membrane filtration process under cross-flow mode 7
2.1.3 Membrane fabrication 7
2.1.4 Surface modification: LPCVD 8
2.1.5 The feature of the coating layer 9
2.2 Membrane fouling 9
2.2.1 Fouling mechanism 9
2.2.2 Foulant sodium alginate 10
2.3 Membrane characterization 12
2.3.1 Water permeability 12
2.3.2 Critical flux 13
2.3.3 Zeta potential and isoelectric point 13
2.3.4 Molecule weight cut off 14
2.3.5 Surface roughness 15
2.4 Membrane cleaning 15
2.4.1 Backwash 15
2.4.2 Chlorine cleaning 16
3 Materials and Methods 17
3.1 Membrane preparation 17

3.2 Overview of the experiments 18
3.3 Foulant solution preparation and characterization 19
3.4 Sodium hypochlorite solution preparation 19
3.5 Membrane characterization by Carman-Kozeny Model 19
3.6 Fouling mechanism 21
3.7 Experimental setup and experimental process 21
3.8 Backwash and fouling resistance 24
4 Results and discussion 25
4.1 Characterization of solution 25
4.1.1 pH and conductivity measurement 25
4.1.2 Size distribution of foulant solution 26
4.1.3 Zetapotential of foulant solution 27
4.2 Chemical stability test 29
4.3 Carmen-Kozeny model estimation 30
4.4 Fouling experiments 31
4.4.1 Influence of calcium under normal flux for artificial solution 31
4.4.2 Influence of flux for artificial water 35
4.4.3 Influence of flux during filtration of surface water 36
4.5 Backwash and fouling resistance analysis 37
4.5.1 Backwash recovery and efficiency comparison 37
4.5.2 Gel layer image 40
4.5.3 Fouling resistance comparison 42
5 Conclusions, limitations and recommendations 45
5.1 Conclusions 45
5.2 Limitations 47
5.3 Recommendations 48
6 References 49

7 Appendix.....56

7.1 The backwash fluxes applied on experiments.....56

7.2 The SEM image of membrane H.....57

7.3 The fouling test for determining the used SA concentration under flux of 345 LMH 58

7.4 The fouling test for determining the used SA concentration under flux of 170 LMH 59

List of figures

Figure 1 Membrane filtration spectrum[24] 5
Figure 2 Membrane structure illustration[27].....6
Figure 3 Different types of membranes: Flat, (multichannel)tubular and hollowfiber membranes from Taizhou Leo Environmental Protection & New Materials Co., China, Fraunhofer IKTS, Germany and Deltapore, Netherlands respectively.....6
Figure 4 Tubular membrane filtration process illustration 7
Figure 5 Schematic of the LPCVD system for SiC layer coating[8].....9
Figure 6 Four fouling mechanisms developed by Hermia (1982)[40] 10
Figure 7 The chemical structures of alginates, chain formation and blocks[46].....11
Figure 8 The egg box model formatting by bind Ca^{2+}[21].....11
Figure 9 The EDL illustration of negatively charged surface.....14
Figure 10 The oxidation process of alginates by NaClO[80] 16
Figure 11 Schematic view of the experimental setup 22
Figure 12 The picture of experimental setup 23
Figure 13 size distribution of 300 mg/L sodium alginate solution 26
Figure 14 size distribution of 300 mg/L sodium alginate solution with 0.5 mmol/L of Ca^{2+} .27
Figure 15 size distribution of 300 mg/L sodium alginate solution with 2 mmol/L of Ca^{2+} 27
Figure 16 Zetapotential of four different types of foulant solution 28
Figure 17 Water permeability change after NaClO soaking.....29
Figure 18 The normalized permeability and pressure to time curve of membrane P (the pristine membrane), L (coated membrane under 750 °C for 60 min) and H (coated membrane under 860 °C for 30 min) when filtrating 31 mg/L SA (up), 31 mg/L SA with 0.5 mmol/L Ca^{2+} (middle) and 31 mg/L SA with 2 mmol/L Ca^{2+} (bottom) solution under normal flux around 170 LMH.....34
Figure 19 The normalized permeability and pressure to time curve of membrane P and membrane H under flux of 170 LMH and 65 LMH using 31 mg/L SA with 2 mmol/L Ca^{2+} as foulant solution 35
Figure 20 The normalized permeability and pressure to time curve of membrane P and membrane H under flux of 170 LMH and 65 LMH using surface water after 5 micron's cartridge filter.....37
Figure 21 The backwash recovery of membranes fouled under normal flux (170 LMH) with backwash flux from 344 to 375 LMH.....39

Figure 22 The backwash efficiency of membranes fouled under normal flux (170 LMH) with backwash flux from 344 to 375 LMH 39
Figure 23 The backwash recovery (left) and efficiency (right of membrane P fouled under lower flux (65 LMH) with backwash flux of 191 LMH 40
Figure 24 The images of gel layer washed out from membrane P when backwash pressure of 6 bar and backwash flux of around 680 LMH was applied (up left: 20X; up right: 20X; bottom left: 40X; bottom right: 80X) 41
Figure 25 Fouling resistance of different types of membrane for the 1st cycle when filtering 31 mg/L SA (up left), 31 mg/L SA with 0.5 mmol/L Ca^{2+} (up right), 31 mg/L SA with 2 mmol/L Ca^{2+} (bottom left) solution under normal flux around 170 LMH and 31 mg/L SA with 2 mmol/L Ca^{2+} (bottom right) solution under lower flux around 65 LMH 42
Figure 26 Fouling resistance of different types of membrane for the 1st cycle when filtering surface water under normal flux around 170 LMH (left) and under lower flux around 65 LMH (right) 42
Figure 27 SEM image of membrane L after 200 h of soaking in NaClO solution 57
Figure 28 Membrane P filtering 7 mg/L SA solution with backwash pressure of 5 bar, duration of 5 minutes and final chemical cleaning with 0.5 % NaClO in ultrasound for 30 minutes 58
Figure 29 Membrane P filtering 7 mg/L SA solution with 2 mmol/L of Ca^{2+} with backwash pressure of 5 bar, duration of 5 minutes 58
Figure 30 Membrane P filtering 30 mg/L SA solution 59
Figure 31 Membrane P filtering 30 mg/L SA solution with 0.5 mmol/L of Ca^{2+} with backwash pressure of 3 bar, duration of 5 minutes 59
Figure 32 Membrane P filtering 10 mg/L SA solution with 0.5 mmol/L of Ca^{2+} with backwash pressure of 3 bar, duration of 5 minutes 60
Figure 33 Membrane P filtering 10 mg/L SA solution with 2 mmol/L of Ca^{2+} 60
Figure 34 Membrane P filtering surface water without any pre-treatment with backwash pressure of 6 bar, duration of 5 minutes 61

List of tables

Table 1 The information of three types of membrane used for study.....17
Table 2 The overall experiments on three types of membrane.....18
Table 3 The relationships between ΔP and filtration time under constant flux mode.....21
Table 4 pH and conductivity value of the solution used for experiments 25
Table 5 The linear regression of the membrane irreversible resistance according to time.....44
Table 6 The backwash fluxes applied on each experiments.....56

List of Acronyms

ALD	Atomic layer deposition
BWP	Backwash pressure
BSA	Bovine serum albumin
CVD	Chemical vapor deposition
CVI	Chemical vapor infiltration
HA	Humic acid
IEP	Isoelectric point
LPCVD	Low pressure chemical vapor deposition
MF	Microfiltration
MWCO	The molecule weight cut off
NF	Nanofiltration
NOM	natural organic matter
PA	Polyamide
PE	Polypropyleneand
PES	Polyethersulfone
PVDF	Polyvilidenefluoride
PZC	Point of zero charge
SA	Sodium alginate
SFR	Specific filtration resistance
TMP	Transmembrane pressure
UF	Ultrafiltration

1 Introduction

1.1 Research context

Water scarcity and pollution have become an increasingly important issue since last century due to the rapid population growth and industrialization process. During this period the global water demand increased by almost six times, forcing people to focus on the water resource protection and water treatment[1]. The reuse, recycling and recovery of waste water after treatment can partly relieve the tense water consumption and reduce the environmental pollution. Conventional water treatment technologies were gradually developed such as coagulation/flocculation, filtration, chlorine disinfection and ion exchange[2, 3]. Membrane filtration, which can be categorized from materials in polymeric and ceramic membrane technologies, is considered an effective method due to its efficient separation capability, less environmental impact and lower energy demand[4]. Currently, polymeric membrane is still the dominate type for water and waste water industries because of its lower price and higher portability. However, its hydrophobicity and low chemical stability decrease its lifespan and limit its performance. Ceramic membrane, in the contrary, has higher mechanical, chemical and thermal stability. Other advantages are that ceramic membranes usually show higher hydrophilicity, which means it can maintain higher flux at low pressure and suffer less from fouling problem. These features prolongs its lifetime, making it suitable for many industrial applications like food and beverage industries, which need frequent cleaning cycle during processing[5]. Ceramic membranes are usually made up of metal oxides (Al_2O_3, TiO_2, ZrO_2) or carbides (SiC), and among them alumina (Al_2O_3) is the commonly applied one due to its low price and good performance[5]. Silicon carbide (SiC), despite its excellent performance on fouling resistance and better hydrophilicity than alumina, shows much less market share owing to its high product prices, which results from its high sintering temperature of around 2000°C during the fabrication process. Additionally, SiC membranes usually have larger pore size than other materials and there is still no reported modification of the pore size of silicon carbide membrane until nanofiltration (NF) scale by solid particle sintering[6].To reduce the fabrication cost of SiC membrane with much smaller pore size, surface modification has been applied. Its idea is to coat a SiC layer, which has lower fouling potential, on top of the pristine Al_2O_3 membrane, which has higher fouling potential but a lower fabrication price. There are many surface modification methods like sol-gel, dip coating, chemical vapor deposition (CVD) and atomic

layer deposition (ALD). while the mainly used method for microporous membrane preparation is sol-gel[7-10]. However, this method is unsuitable for coating a SiC layer on Al_2O_3 pristine membrane because the high sintering temperature of SiC (2000 °C) will melt the Al_2O_3 support (1000 °C). To fabricate a 'perfect' SiC layer under a lower temperature, while reducing its pore size possibly close to NF scale, low pressure chemical vapor deposition (LPCVD) has been applied to develop SiC-Al_2O_3 ultrafiltration membranes with appropriate deposition time[8, 11].

The fouling problem and chemical resistance to the cleaning solutions are two main problems that determine the lifespan of a ceramic membrane. Considerable filtration experiments have been done on ultrafiltration and nanofiltration membranes with SA and NOM (natural organic matter, which can represent the surface water): Moyo et al. did fouling researches of SA, HA and BSA on TiO_2-Al_2O_3 membrane and found out in the early stage of filtration process, the fouling on membrane surface was mainly controlled by interactions between membrane surface and the foulant solution[12]; Angelis did SA, HA and BSA fouling experiments on Fe_3O_3 UF membrane and concluded that fouling was first controlled by membrane-foulant interactions as well, and membrane surface and solution pH influenced the irreversibility of the fouling layer[13]; Zhang et al. studied the effect of Ca^{2+} on the fouling of SA and suggested that as the increase of Ca^{2+}, intermolecular binding of Ca^{2+} by alginate rather than intramolecular occurred first, which explained the unimodal pattern of the filtration resistance and the specific filtration resistance (SFR)[14]; van der Blink studied the influence of Ca^{2+} on the fouling of alginate and found out that with the increase of Ca^{2+}, the fouling rate increase largely and the reversibility decreased to 3%[15]; Li et al. did fouling experiments with NOM on negatively charged polymeric membrane and found out that: the Ca^{2+} bridged between NOM and the membrane surface and caused heavy fouling, and the backwash with demineralized water was more efficient because the bridging effect was reduced[16, 17]. Researches on the fouling of other types of foulant were also done on SiC membrane: Hofs et al. compared the fouling of ceramic and polymeric MF membranes by lake water and found out that polymeric had less reversible fouling while SiC membrane had less irreversible fouling[18]; Arndt et al. compared the influences of operation mode, presence of Ca^{2+} and crossflow velocity on SiC-Al_2O_3 and Al_2O_3 membrane treating sodium alginate (SA) solution, and concluded that during the crossflow filtration, cake filtration dominant the mechanism, and Ca^{2+} concentration was found to greatly impacted the removal of fouling layer by shear force[19]; Chen et al. studied the fouling by oil-in-water emulsion on SiC-Al_2O_3 membrane fabricated

by LPCVD under 750 °C and found out that this new type of membrane had better antifouling ability than pristine alumina membrane[8], and this ability was favoured by increasing pH and decreasing Ca^{2+} concentration of foulant solution[11]. However, gap remains that for silicon carbide-alumina membrane fabricated by LPCVD under higher temperature (860 °C), the membrane feature haven't been studied yet. Therefore, fouling tests with different kinds of foulants and chemical stability tests on possibly used chemical cleaning solution should be done on the newly fabricated ceramic membrane to evaluate its antifouling ability and the market value.

1.2 Research objectives and questions

The objectives of this study are to analyse the chemical stability, fouling features and the backwash efficiency of the SiC-Al_2O_3 ultrafiltration membrane fabricated using LPCVD method under different temperatures. The research questions are as follows:

a) Will the SiC membrane coated under different temperatures remain stable in the 1% and 5% NaClO solution?
b) What is the fouling of SiC coated membrane against sodium alginate compared with pristine alumina membrane?
c) What is the backwash efficiency on SiC coated membrane compared with pristine alumina membrane?
d) What is the influence of the addition of Ca^{2+} on the fouling features and the backwash efficiency?
e) What is the influence of flux change on the fouling and the backwash efficiency?

And the research hypothesis is that the SiC coated membrane remains stable in a NaClO solution due to the excellent chemical stability of this material[20]. The SiC coated membrane has better performance than the pristine during the fouling tests against a sodium alginate solution and surface water because of the electrostatic repulsion force between the SiC membrane surface and the foulant solution. For both membranes the fouling mechanisms are expected to be pore blocking and cake filtration like the finding by Chen et al., Arndt et al. and Moyo et al. [8, 12, 19]. The SiC coated membrane should have a better backwash efficiency compared with the pristine membrane due to the better antifouling ability than the pristine membrane. After the addition of Ca^{2+}, the advantage of the antifouling performance of the coated membrane alleviate due to the decrease of the repulsion force between SiC surface and the foulant solution[21]. Both the addition of

Ca^{2+} and the decrease of the flux are expected to increase the backwash efficiency because the irreversible fouling caused by the strong membrane-foulant interaction was reduced and the transport of the foulant to the membrane was reduced[15].

1.3 Research approaches

To accomplish the objectives and study the research questions listed above, the research was divided into several parts:

a) Theoretical background

In this part, a brief introduction to the ceramic membranes, filtration process was given to clarify the principle of how the ultrafiltration membrane works to produce clean water. In addition, information about membrane fouling, foulants and parameters that could influence the fouling process was offered. Further, information was givenabout membrane cleaning, including the hydraulic cleaning and chemical cleaning methods used in this study.

b) Materials and methods

This part shows how the whole experiment was designed, including the introduction to how the membrane, foulant solution and cleaning solution were prepared. Information about the analytical methods on solution and membrane characterization was provided as well. The mathematical models used for pore size estimation and fouling mechanism analysis were listed to how the fouling was quantified.

c) Results analysis

The results on solution characterization, including pH, size distribution and zeta potential analysis were listed first. Then came the results of the chemical stability tests and fouling experiments of three types of membrane with four types of foulant solution. The fouling curves, backwash efficiency and fouling resistance were analysed and possible explanations were offered.

2 Theoretical background

2.1 Ceramic membrane filtration

Membrane for filtration is usually made up of polymeric material or ceramic material. The most applied and well-studied one is polymeric membrane, which is usually fabricated by hydrophobic polymers like polyamide (PA), polypropylene (PE), polyethersulfone (PES) and polyvilidenefluoride (PVDF). The history of the ceramic membrane dates back to almost a century ago, and the first commercial application of UF membrane for liquid separation was in 1980s[22]. Even though the capital cost of ceramic membrane is relatively high, this kind of membrane outstands others on the filtration under extreme conditions like large alkalinity and high temperature because of its advantages of great physical and chemical stability. Therefore, ceramic membrane filtration now plays an important role not only in food and beverage industry, but also pharmaceutical industry, petrochemical industry and chemical industry[22, 23]. As shown in Figure 1, different pore sizes of the membrane targets at different materials with increasingly smaller size.

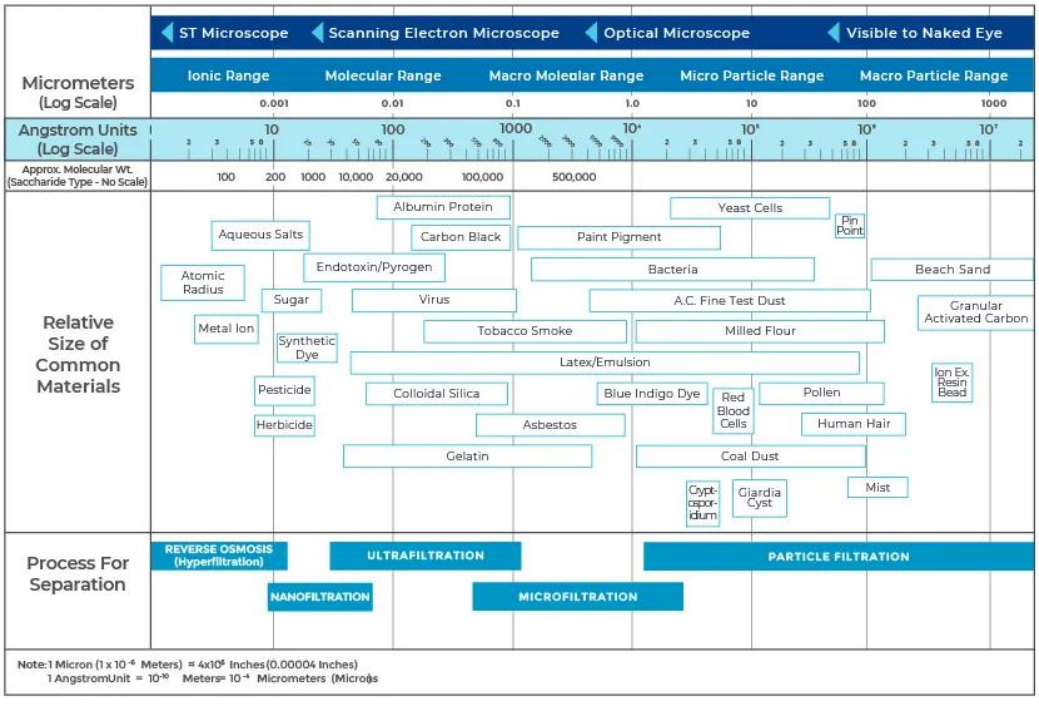

Figure 1 Membrane filtration spectrum[24]

2.1.1 Membrane structures and configurations

To better understand the membrane filtration, it's necessary to have an overview of the membrane structure. Generally the ceramic membranes for water treatment contain three parts: a selective layer, an intermediate layer(s) and a support layer[5]. A selective layer is a thin layer which fulfils the separation job during the filtration process and identifies the filtration as microfiltration (MF), ultrafiltration (UF) or nanofiltration (NF); intermediate layers help prevent the high resistance resulted from the penetration of small particles through the coarse support layer; a support layer contributes to the mechanical strength and functions as the support for the whole membrane[25]. The configuration of ceramic membrane can be either cylindrical (hollow or tabular) or flat depending on different application situations[26].

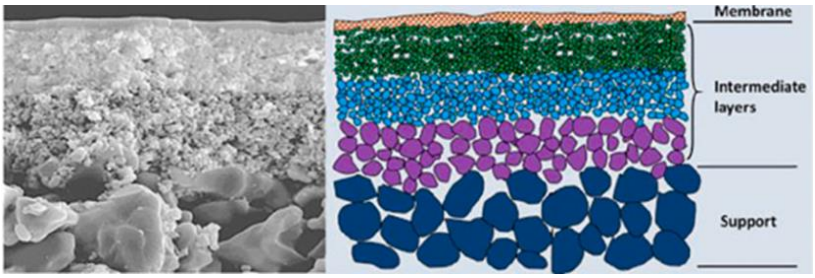

Figure 2 Membrane structure illustration[27]

Figure 3 Different types of membranes: Flat, (multichannel)tubular and hollowfiber membranes from Taizhou Leo Environmental Protection & New Materials Co., China, Fraunhofer IKTS, Germany and Deltapore, Netherlands respectively

The most common materials used for the fabrication of ceramic membrane for water treatment are alumina (Al_2O_3), titania (TiO_2), zirconia (ZrO_2) and silicon carbide (SiC) [28]. Usually MF membranes with pore size larger than 100 nm are made of α-alumina, and zirconia and titania are used to made UF membranes with the pore size from 20 nm to 100 nm and with molecular weight cut off from 1 kDa to 5 kDa respectively[22].

2.1.2 Tubular membrane filtration process under cross-flow mode

In this research, tubular membrane with single channel was used for filtration test. For this kind of membrane, the filtration process can be illustrated in the Figure 4 below. The feed solution is pumped into the channel of ceramic membrane with relatively high pressure to form transmembrane pressure (TMP), a pressure difference between the inlet and outlet part of the membrane. TMP acts as driving force to help the feed water penetrating through membrane to produce clean permeate at the outside part and meanwhile the selective layer of the membrane decides on the size of particles can pass. Then the left water together with the contaminants at another end of the membrane becomes concentrate with less amount of water and higher concentration of contaminants. The concentrate will be cycled back to the feed water tank to form a circulation loop and this is called the cross-flow mode with recycled flow.

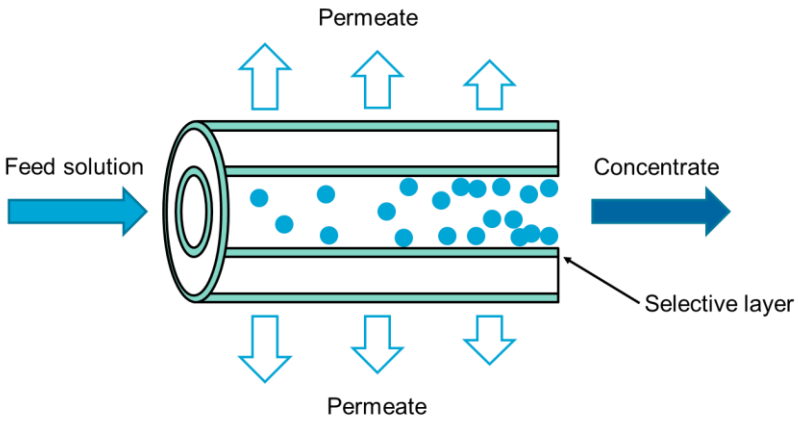

Figure 4 Tubular membrane filtration process illustration

2.1.3 Membrane fabrication

To fabricate a porous ceramic membrane with pore size larger than 1 μm, several steps are needed: preparation of ceramic powder paste, shaping and heat treatment (calcination and sintering)[29]. To have membrane pore size further narrow down, pore structure gradients are necessary among three layers in the membrane and methods like sol-gel, dip-coating, CVD and ALD are needed[30].

Despite the outstanding mechanical, thermal and chemical features of SiC membrane, one main disadvantage of the SiC membrane is that its build-up cost is relatively high due to its

sintering temperature of approximately 2000 °C needed for the formation of the strong covalent Si-C bonds [23, 31-34]. Challenges still exist on coating thin layers of SiC with pore size smaller than 100 nm by solid particle sintering, and this limits the SiC application in water treatment[6]. To avoid the high temperature during the sintering process when fabrication the SiC membrane, surface modification methods has been considered to coat SiC layer on the microporous supports by CVD/CVI or dip coating deposition[6, 32, 35].

2.1.4 Surface modification: LPCVD

Compared with dip coating, CVD method can produce denser structure on the support membrane, resulting in lower permeability, which is suitable for gas separation[32]., By using CVD methods, the pore size of fabricated membrane can be narrow down to smaller than 1 nm[36]. A thick layer of SiC can be coated on α-alumina or SiC membrane support first under 700-800 °C with one or two precursors and then 1000 °C in Ar for calcination[32, 35]. The first reported preparation of nanoporous SiC membrane on γ-alumina tubular membrane for H2 selection was done by Ciora et al. using CVD, but still with high-temperature post treatment to improve the H_2/H_2O selectivity and H_2 permeance[32]. With the realization of the experimental fabrication of unltrathin SiC membrane as substrate platform for cell culture by LPCVD[37], new trails have been done on coating SiC on α-alumina membrane using LPCVD to fabricate UF membrane for water treatment with high water permeance by Chen et al for oil-water emulsion treatment[8]. In his fabrication process, dichlorosilane (SiH_2Cl_2) and acetylene (C_2H_2) diluted at 5% in hydrogen (H_2) were used for precursor and the LPCVD system was shown in Figure 5[8]. In our research, this method was used to produce SiC-Al_2O_3 UF membrane but under higher temperature of 860 °C.

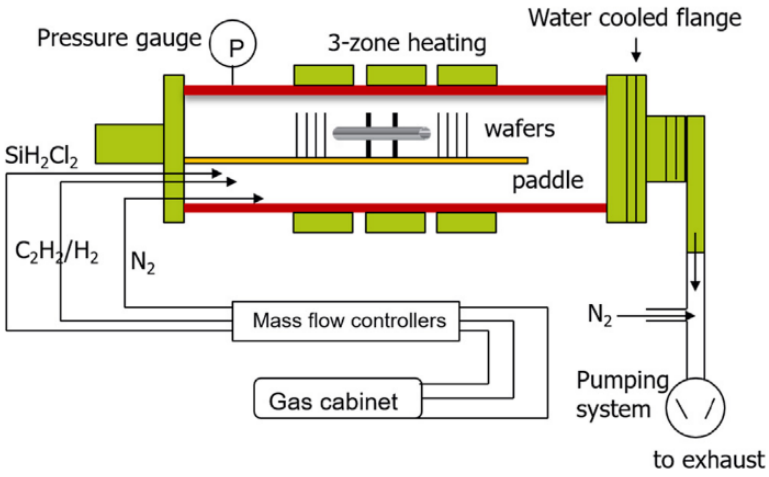

Figure 5 Schematic of the LPCVD system for SiC layer coating[8]

2.1.5 The feature of the coating layer

After the process of LPCVD, a new SiC layer can be coated on top of the Al_2O_3 pristine membrane to act as the selective layer with relatively good water permeance[8]. According to the literature, the zetapotential of SiC was around -40 mV to – 20 mV while for Al_2O_3 was around 10 mV to 40 mV when the pH of the solution was neutral[38, 39]. However, same types of Al_2O_3 membrane used as pristine in this experiment was tested to have a zetapotential of around -17 mV at pH of 6.7 by Chen et al.[11].Therefore, this negative zetapotential was used for analysis. The zetapotential difference between Al_2O_3 and SiC indicates that when the foulant solution shows negative zetapotential, there would be a stronger repulsion force between SiC layer and the foulant solution than that for Al_2O_3 membrane. Therefore, the antifouling ability of SiC coated membrane is expected to be better than the pristine Al_2O_3 membrane. Additionally, the SiC material itself has a good chemical stability and will only react with chlorine when temperature is above 900°C[20]. Consequently this membrane should be highly resistant to the NaClO cleaning under room temperature.

2.2 Membrane fouling

2.2.1 Fouling mechanism

Membrane fouling is a process of foulant accumulation on top or in the pores of the membrane. Fouling mechanisms were developed to mathematically describe the principle of fouling. According to Hermia (1982), there are altogether four types of fouling mechanisms (Figure 6): complete blocking, intermediate blocking, cake filtration and standard pore blocking[40]. Complete blocking means the particles only deposit on the unobstructed membrane

surface but are not allowed to deposit on top of each other; the intermediate blocking resembles that the particles have possibility to deposit on top of each other on the base of complete blocking; cake filtration is that the particles form several cake layers on the membrane surface and the water permeability decreases with the layer thickness increasing; the standard pore blocking means the particles deposit on the walls of the pores and gradually clog up the passage[40].

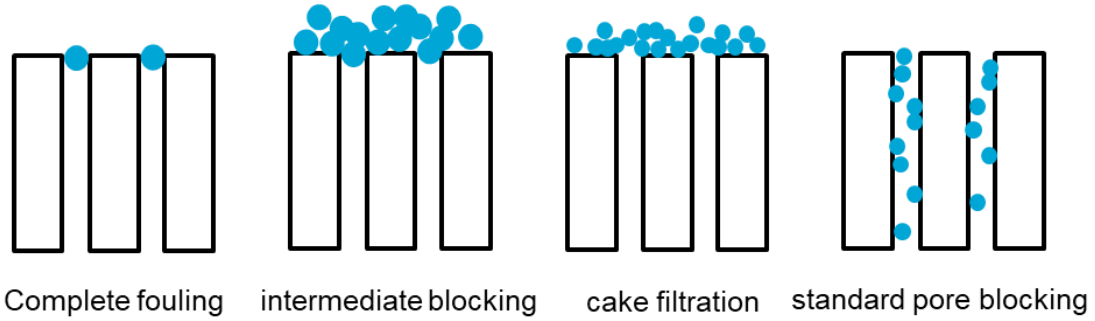

Figure 6 Four fouling mechanisms developed by Hermia (1982)[40]

The corresponding mathematical models are listed in 3.6. Since Hermia's model was raised under the constant pressure dead-end filtration mode, adaptions should be made to fit in the constant flux mode in this study.

2.2.2 Foulant sodium alginate

This research intended to use sodium alginate as foulant. Alginates are polysaccharides (polymers which contain chains of carbohydrates linked together via glycosidic bonds) which naturally occur in, produced and refined from brown algae genera including *Alaria*, *Ascophyllum*, *Cystoseira*, *Ecklonia*, *Eisenia*, *Fucus*, *Laminaria*, *Lessonia*, *Macrocystis*, *Nereocystis* and *Sargassum*, with *Macrocystis pyrifera* and *Ascophyllum nodosum* being the major resources[41, 42]. For the brown algae, alginates mainly present in the cell wall and provide it with flexibility and mechanical strength in the water likewise cellulose functioning as the structuring component for terrestrial plants[43]. In the seaweed it usually exists in the form of metal salts like sodium and calcium alginate in the cell wall and intercellular regions. It can also be synthesized as exopolysaccharide by some bacteria like Azotobacter vinelandii or the mucoid strains of *Pseudomonas aeruginosa* to enhance the function and the structure of the biofilm[44]. Consequently it is considered as the determinants of its physicochemical properties[45].

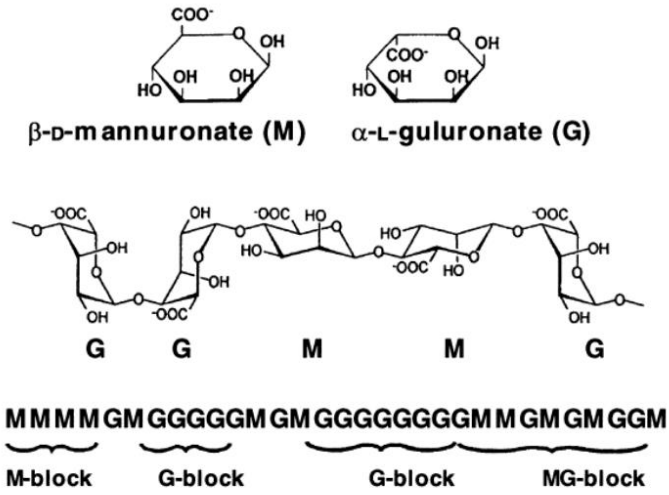

Figure 7 The chemical structures of alginates, chain formation and blocks[46]

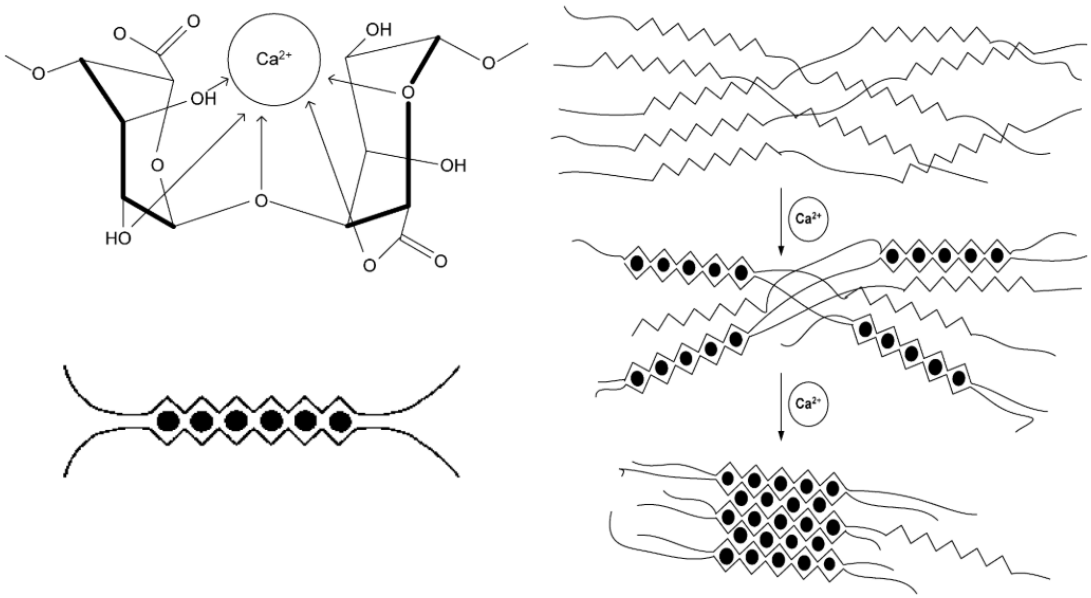

Figure 8 The egg box model formatting by bind Ca^{2+}[21]

Alginates (Figure 7) are comprised of 1,4-β-D-mannuronic acid (M) and 1,4-α-L-guluronic acid (G) monomers, which form homopolymers (MM or GG) or heteropolymers (MG or GM) via o-glycosidic bonds[41, 47]. Since the pKa value of mannuronic acid and guluronic acid are low (3.38 and 3.65 respectively), alginate under neutral pH becomes polyanionic [48, 49].The M/G ratio and their sequence vary between different species and even different parts of the same species, impacting the physical and chemical properties of the alginates: more G-blocks (polyguluronic blocks) increase the rigidity and density of the gel while M-blocks (polymannuronic blocks) increase its flexibility and porosity[50-52]. Among these

two homopolymers, the G-blocks were found to have a high affinity for Ca^{2+} so it bounds this divalent ion between two chains, which align the G-blocks and form an 'egg-box' model (Figure 8) [53, 54].

The gelation process can be categorised into two types: external gelation and the internal gelation[55, 56]. In the external gelation procedure, the gelling ions (e.g. Ca^{2+}) are available directly to the carboxylic groups of guluronic acid in the alginate, through which the hydrogel is formed irreversibly due to ion diffusion[55]. As for the internal gelation, the gelling ions originates from an insoluble sources and are available to the alginate after dissolution process which lowers the pH[56]. The released H^+ replaces some of the crosslinked Ca^{2+} and lead to more porous and homogeneous gel matrices[57, 58].

Sodium alginate, the most common alginate salt which is soluble in water, has been widely applied in many industries such as food, beverage, fertilisers, textile, printing and pharmaceuticals due to its property of swelling, thickening and increasing viscosity[41, 42, 46]. It is often considered as the model foulant for extracellular polymeric substances (EPS),which is produced by microorganisms and are mainly made up of polysaccharides, nucleic acids and proteins[59]. Since EPS is one of the main causes of membrane fouling in micro and ultrafiltration of surface water and waste water, sodium alginate is frequently used for filtration and fouling characteristics test[19, 60].

2.3 Membrane characterization

2.3.1 Water permeability

To quantify the ability of a membrane to filtrate the feed solution, water permeability P_w [LMH/bar] was commonly used. It can be calculated as the litres of water this membrane can filtrate on 1 m^2 of filtrating area within an hour under 1 bar of transmembrane pressure (TMP). The equation is shown below:

$$P_w = \frac{J}{TMP} = \frac{Q_p}{A \times TMP} \qquad \textit{Equation 1}$$

J stands for the water flux and it can be calculated from the permeate flow Q_p [mL/min] and membrane filtration area A [m^2]. TMP [bar] standards for the transmembrane pressure and it means the pressure difference between the membrane filtrating side and the permeate side. It can be calculated from the pressure of the feed solution side P_f [bar], the pressure of the concentrate side P_c [bar] and the pressure of the permeated side P_p [bar]. The equation is shown below:

$$TMP = \left(\frac{P_f + P_c}{2}\right) - P_p \qquad \textit{Equation 2}$$

Since the permeate side is usually connected to the air pressure, the P_p part can be omitted when pressure gauge showing the pressure difference between flow and atmosphere is used.

2.3.2 Critical flux

When operating a ceramic membrane system, flux decline happens due to the fouling of the membrane. An important approach to reduce the flux decline is to operate the filtration system below the critical flux. Critical flux is defined as a flux above which the membrane fouls heavily and below which only negligible fouling occurs on the membrane. Two types of critical flux: strong form and weak form, were described by Wu et al.[61]. A strong form of critical flux exists at the limit of flux when the suspension flux and clean water flux are equal under a given TMP. This critical flux can be recognized when the TMP starts to deviate from the linear relationship with flux[62]. For a weak form of critical flux, it exits when the TMP and flux are in linear relationship but its slope is lower than the slope of TMP to flux when filtering clean water[63]. For filtration under constant flux mode, the critical flux is recognized by researches as the change of pattern of TMP to time curve[11, 64, 65].

2.3.3 Zeta potential and isoelectric point

When exposed to a certain liquid, the membrane material naturally shows surface charges and it influences the distribution of ions provided by this liquid in the interfacial area. This phenomenon is explained by electric double layer (EDL) structure. As shown in Figure 9, if the material shows negative charges in the solution, the cations will be strongly attracted to the region surrounding the material surface and form a stable layer called stern layer. The anions, which carry negative charges, will be repelled from the surface and can only gather loosely at longer distance than the stern layer. This layer is less firmly bounded to the material surface by electric force and it forms the second layer called diffusion layer. The outer boundary of this layer is slipping plane and it entitizes the ions and the material particle beneath. When the material particle moves due to gravity, the ions inside the slipping plane will move with it thus separating the attached fluid from the mobile fluid. The electric potential measured on this plane is zeta potential (ζ) and it shows the potential difference of the surrounding medium and the stationary fluid layer associated to this particle.

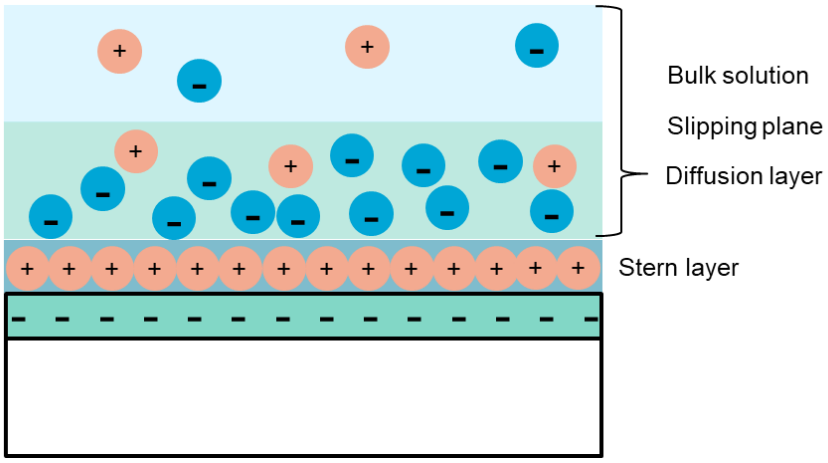

Figure 9 The EDL illustration of negatively charged surface

Isoelectric point (IEP) is another value that quantify the surface charge of the material in the scale of pH value. When placed in the water of different pH, the surface attracts H^+ or OH^- to balance the charge. Under a certain pH these is no net charge observed on the material surface, this pH value is defined as IEP , which can be obtained from electrokinetic measurements. For ceramic materials, their isoelectric point (IEP) can be important as it shows the pH at which there are no net electrical charges on the material-water surface: if the solution pH is higher than the isoelectric point, the surface charge of the membrane will be negative due to the loss of protons to the solutions; if the solution pH is below the IEP then the membrane will be positive. Alumina membranes are the most commonly applied ones compared to other membranes due to its lower price and relatively good performance[5]. It usually has an isoelectric point from 7 to 10[66]. Silicon carbide has the lowest isoelectric point (2.5-3.5) among these materials, indicating the highest negative charge at neutral pH. Together with larger hydrophilicity and stronger chemical resistance in harsh and aggressive environments, SiC shows excellent fouling resistance than other materials[18, 23].

2.3.4 Molecule weight cut off

The molecule weight cut off (MWCO) of a ceramic membrane is a parameter that describes the quality of membrane to reject foulant particles. It shows the value of lowest molecular weight of solute that 90% of which is rejected by the membrane.

2.3.5 Surface roughness

Surface morphology plays a key role in fouling performance of the membrane. From the microscopic view, fouling forms due to the interactions between foulant molecules and the uneven membrane surface. These molecular interactions contribute to the foulant adhesion and the foulant layer formation, which are two main causes of the irreversible fouling[67, 68]. Researches have been done on the influence of surface roughness on foulant sodium alginate: Hashiona et al. (2011) showed that rougher membrane made of cellulose acetate butyrate polymer has better antifouling ability against sodium alginate[69]. According to Hashiona et al. (2011), sodium alginate foulants tend to accumulate in the valley part of the membrane surface, which ensure rougher membrane of better antifouling ability [70]. Li et al. (2019) theoretically proved that rough membrane is less likely to adhere the sodium alginate than smooth membrane due to the higher bending energy[71].

2.4 Membrane cleaning

The cleaning of membrane helps to recover its water permeability after fouling to prolong its working time and ensure its working efficiency. Usually there are two types of cleaning methods: physical cleaning and chemical cleaning. The most common physical cleaning methods is backwash. By using the permeate or demineralized water, the reversible fouling on the membrane will be flushed out by flux under higher pressure.

2.4.1 Backwash

Backwash is one type of hydraulic cleaning methods that reverses the flow to loosen or remove the cake layer and the foulant particles in the pores from the membranes[72]. Backwash can be manipulated by changing the operational pressure and the type of backwash solution used. The pressure used decides the backwash flux, and the commonly used flushing flux is 2-3 times of the working flux during filtration[18, 72]. The composition of the backwash solution is vital for an efficient cleaning. Considerable studies shown that demiwater has better effect than the permeate due to its capacity to take ions from the foulant layer[73]. For the backwash efficiency of SA-fouled membrane, the divalent cations in the backwash solution had negative influence on the cleaning efficiency while the NaCl solution greatly increase the efficiency[74]. For the backwash of NOM fouled membrane, demineralized water

was more effective as it alleviated the bridging effect between Ca^{2+} and NOM even though the influence was limited[16, 17].

The backwash efficiency is also influenced by the duration and the frequency of the backwash[75]. If the interval of backwash is too long, then the fouling layer will be compacted on the membrane, which becomes hard to remove[76, 77]. The duration of the backwash influences the backwash by that: if the duration is too short, then the foulant cake can only be expanded rather than washed out, and the expanded cake layer will be compressed back in the next filtration cycle; if the duration is too long, it will be a waste of backwash solution and the energy with little increase on the backwash efficiency[78, 79].

2.4.2 Chlorine cleaning

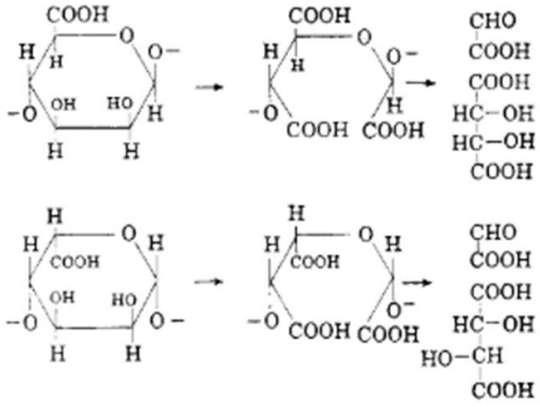

Figure 10 The oxidation process of alginates by NaClO[80]

Chlorine is an intensive chemical used for membrane cleaning and disinfection. It removes the fouling of alginates by the principle of oxidation (Figure 10). The chlorine will cleave the C-C bond which helps keeping the ring structure and finally oxidize the alginates into acids with smaller chains which can dissolve into the solution. NaClO solution. NaClO solution was introduced in the backwash water in many cases to reduce the fouling on the membrane[81, 82]. It shows good water permeability recovery for model foulants of polysaccharides and protein, while it is less effective for removing the fouling of humic substances[83]. The chlorine has better performance at lower pH around 7[84].

3 Materials and Methods

3.1 Membrane preparation

In total three different types of single tubular ceramic membranes were prepared for fouling tests and chemical stability tests: pristine membranes (P), lower temperature coated membrane (750 ^{o}C, L) and higher temperature coated membrane (860 ^{o}C, H). The pristine membranes were porous alumina tube (100nm) purchased from the company Coorstek. The last two types of membranes were surficially modified from the pristine membranes using the LPCVD method: one type was coated under 750 °C for 60 minutes and the other under 860 °C for 30 minutes. The corresponding measured thickness of the coating layer growing on wafers were 15.07 nm and 14 nm.

The overall information of these membranes are gathered in Table 1.

Table 1 The information of three types of membrane used for study

Membrane abbreviation	P	L	H
Length [mm]	100	100	100
Inner diameter [mm]	6.98	-	-
Outer diameter [mm]	10.15	-	-
Pore size [nm]	71[1]	55[2]	40[3]
Coating condition	-	750 °C for 60 minutes	860 °C for 30 minutes
Colour	White	Grey	Golden brown

Before coating, the water permeabilities of the pristine membranes were tested without sealing just for quality checking. After that, the pristine membranes were cleaned under 650 °C for 3h (Nabertherm air circulation furnace N30/65HA) to clear the carbon powder left by the O-rings, which would influence the coating performance during LPCVD. After coating, three types of membranes were sealed with LOCTITE® EA 9492 first at both ends of the membrane for 1 cm each and then soaked in the ultrapure water overnight to saturate them with

[1] Data from [59], where the same type of pristine membrane was tested
[2] Data from [59], where the same type of coated membrane was tested
[3] Estimated from Carmen Kozeny model in 4.3

water. Then the formal water permeabilities were tested under constant flux for 10 minutes to obtain an average value.

3.2 Overview of the experiments

In the research, fouling tests and chemical stability tests were done on three types of membranes. Four types of foulant solution were used: 31 mg/L SA solution, 31 mg/L SA solution with 0.5 mmol/L Ca^{2+}, 31 mg/L SA solution with 2 mmol/L of Ca^{2+} and surface water. The chemical stability test was done using 1% NaClO and 5% NaClO solution. More detailed information on experiments was listed in Table 2. When a 'lower flux' was mentioned for the fouling tests, the operational flux was 65 LMH, otherwise a normal operational flux of 170 LMH was applied.

Table 2 The overall experiments on three types of membrane

	Membrane P	**Membrane L**	**Membrane H**
Description	pristine Al_2O_3 membrane	SiC coated under 750 °C for 60 min	SiC coated under 860 °C for 30 min
Chemical stability test	-	1% NaClO 100h 5% NaClO 100 h	1% NaClO 100h 5% NaClO 100 h
Fouling experiments	31 mg/L SA solution	31 mg/L SA solution	31 mg/L SA solution
	31 mg/L SA + 0.5 mmol/L Ca solution	31 mg/L SA + 0.5 mmol/L Ca solution	31 mg/L SA + 0.5 mmol/L Ca solution
	31 mg/L SA + 2 mmol/L Ca solution	31 mg/L SA + 2 mmol/L Ca solution	31 mg/L SA + 2 mmol/L Ca solution
	31 mg/L SA + 2 mmol/L Ca solution (lower flux)	-	31 mg/L SA + 2 mmol/L Ca solution (lower flux)
	Surface water	-	Surface water
	Surface water (lower flux)	-	Surface water (lower flux)

3.3 Foulant solution preparation and characterization

Model solutions and surface water were used for filtration tests. The concentration of the SA solution needed (later turned out to be 31 mg/L) was determined by trial and error to fit the first round of fouling time around 2 hours for the pristine membrane. Then 0.5 mmol/L of Ca^{2+} and 2 mmol/L of Ca^{2+} was dosed into this concentration of SA solution to simulate the water with different concentrations of Ca^{2+}.

For the sodium alginate (SA) solution, 31 mg/L SA solution without Ca^{2+}, 31 mg/L SA solution with 0.5 mmol/L Ca^{2+} and 31 mg/L SA solution with 2 mmol/L of Ca^{2+} were prepared. The stock solution with a concentration of 1 g/L was firstly prepared by mixing SA powder (SIGMA-ALODRICH) and demineralized water. Then different concentrations of SA solutions were made by diluting the stock solution and mixing using a magnetic stirrer overnight. For the SA solution with Ca^{2+}, first certain amount of SA stock solution was pipetted into the container before solution was diluted to 3 L; then certain amount of calcium chloride powder (SIGMA-ALODRICH) was added into the solution before mixing. Surface water from the Schiewater canal was pre-treated using the 5 micron cartridge filter before fouling test.

The zetapotential and particle size distribution (PSD) of all types of foulant solution used for filtration was tested using Zetasizer Nano ZS (Malvern Panalytical) provided by IHE Delft Institute for Water Education. The pH and conductivity of the solution was measured by WTW inoLab_IDS Multi 9420.

3.4 Sodium hypochlorite solution preparation

The sodium hypochlorite solution used for chemical stability test was diluted from 12.5% NaClO solution (Brenntag). For 1% of NaClO solution, 40 mL of 12.5% of NaClO solution was transferred into the 0.5 L of Duran® laboratory bottles and for 5% of NaClO solution, 200 mL of that solution was used and then diluted into 0.5 L. The 1 % and 5 % of NaClO solution was used for chemical stability test and the 1 % of NaClO solution was used for the chemical cleaning of tested membrane.

3.5 Membrane characterization by Carman-Kozeny Model

The average pore sizes of the coated membranes were estimated by Carman-Kozeny equation. This equation was first used to describe the pressure drop of laminar flow along a

packed bed of solids. To describe the pressure drop along the ceramic membranes, the membrane can be considered as a packed bed of near-spherical particles as illustrated by [85]. The Hagen-Poiseuille law was used for the adaption of this equation as it governs the flow velocity for ultrafiltration and microfiltration membrane with ideally cylindrical pore due to their small pore sizes[86]. Since in the real situation the porous membrane may not be ideally cylindrical or straight, further modifications were made on the Carman-Kozeny and the bulk permeability can be calculated by equation below[87]:

$$P_w = \frac{J}{TMP} = \frac{\varepsilon^3}{2(1-\varepsilon)^2 a_v{}^2 \mu \tau l} \qquad \textit{Equation 3}$$

Where J [$m^3/(m^2 \cdot s)$] stands for the permeate flux through membrane; TMP [Pa] is the transmembrane pressure; ε [-] is the porosity of membrane; a_v [1/m] is the specific surface area; μ [Pa·s] is the viscosity of the fluid; τ [-] is the tortuosity factor and l [m] is the layer thickness.

In this study, several assumptions were made to estimate the pore size of the membrane from the water permeability.

a) Since the temperature of water used for permeability test was around 20 °C under the atmospheric pressure of 1 bar, the dynamic viscosity μ used was 0.001 Pa·s.
b) The specific surface area can be calculated from porosity and hydraulic diameter of the membrane

$$a_v = \frac{4\varepsilon}{D(1-\varepsilon)} \qquad \textit{Equation 4}$$

c) The tortuosity was estimated from porosity as suggested by Pisani (2011) for most porous materials[88]. The tortuosity applied in this case was latter calculated to be 1.84.

$$\tau = \varepsilon^{-0.5} \qquad \textit{Equation 5}$$

d) Since the selective layer is responsible for most of the TMP, the lay thickness l was assumed to be the thickness of the selective layer so that an overall porosity can be back calculated. The influence of the coating layer on the porosity was neglected because the thickness increase was 15.07 nm while the selective layer was around 26.7 um. Then the back calculated porosity was fixed when estimating the pore size from the permeability of the coated membrane.

3.6 Fouling mechanism

Fouling mechanism model mathematically describes four types of fouling as mentioned in 2.2.1. Consequently, it is important to recognize the mechanism for better fouling understanding, especially the cake filtration which represents a slow and stable fouling.

Since the fouling mechanism model developed by Hermia (1982) is meant for dead-end filtration under constant pressure, adaptions are made by Kirschner et al. (2019) on the original mathematical model to fit the constant flux crossflow mode. The equations are listed in Table 3.

Table 3 The relationships between ΔP and filtration time under constant flux mode

Fouling type	Corresponding equation
Complete blocking	$\Delta P_t = \frac{\Delta P_0}{(1 - \frac{\sigma J}{B}(1 - \exp(-Bt))}$
Intermediate blocking	$\Delta P_t = \frac{\Delta P_0}{\left(\frac{1}{K_i} + \left(1 - \frac{1}{K_i}\right)\exp(-K_i B t)\right)}$
Cake filtration	$\Delta P_t = \Delta P_0(1 + K_C B t)$
Standard pore blocking	$\Delta P_t = \frac{\Delta P_0}{(1 - K_S a_0 J t)^2}$

In this table, ΔP_t and ΔP_0 means the TMP at time t and initial transmembrane pressure. J [m/s] is the permeate flux applied during filtration process. σ [m^{-1}] standards for the blocked membrane surface area after filtrating 1 m^3 of permeate. B [s^{-1}] is a constant called the particle resuspension rate, which represents the frequency of the removal of the foulant from the membrane surface by the shear force in the cross flow mode. Ki [-], Kc [m^{-1}] and Ks [m^{-3}] are intermediate blocking constant, cake filtration constant and standard pore blocking constant.

3.7 Experimental setup and experimental process

The design of membrane filtration setup under constant flux mode was shown in Figure 11. This setup only contained one pump (Liquiflo Model H7N Heavy Duty Industrial Gear Pump) and a pump drive (Optidrive E3 with part number of ODE-3-140022-3F1B) to extract

the feed solution. Therefore, the constant flux mode was guaranteed by a valve which was controlled by the software. As the fouling happened on the membrane surface, less flux was allowed to pass the membrane and the permeate flow rate decreased. The software detected it via a flowmeter and then automatically closed the valve to increase the pressure on top of the membrane so that more solution would pass through the membrane. Aside from this, another two pressure transducers were connected to the computer as well for the detection of TMP. To fulfil the backwash job, backwash vessel was used and the pressure was provided by the pressed air system in the lab.

The setup used in the water lab was shown in Figure 12.

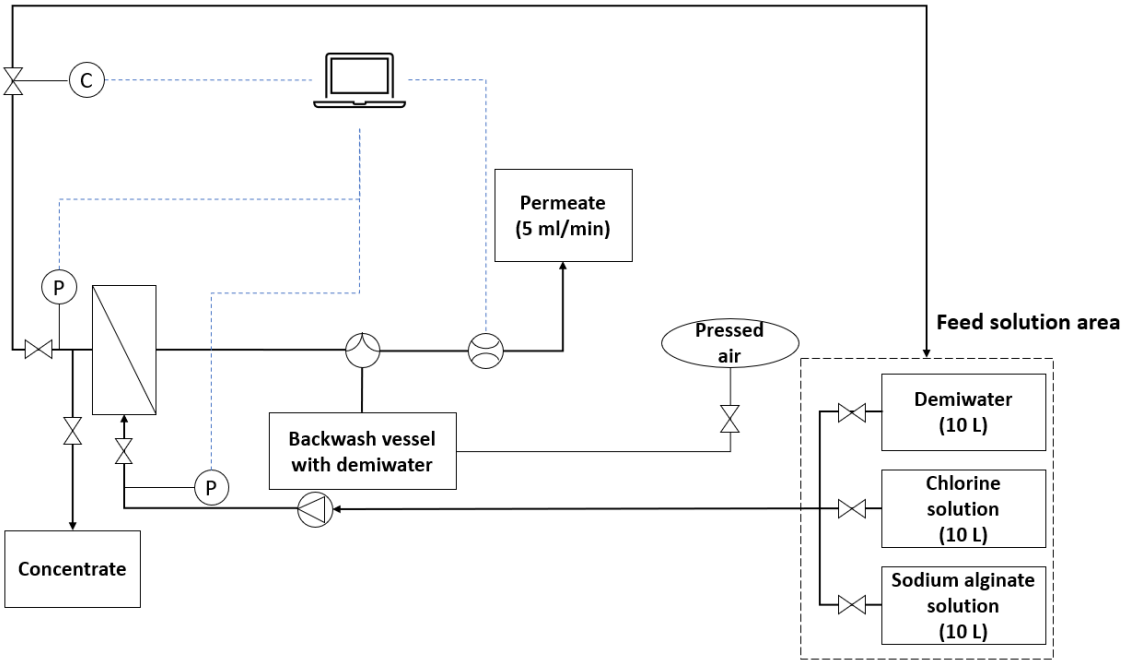

Figure 11 Schematic view of the experimental setup

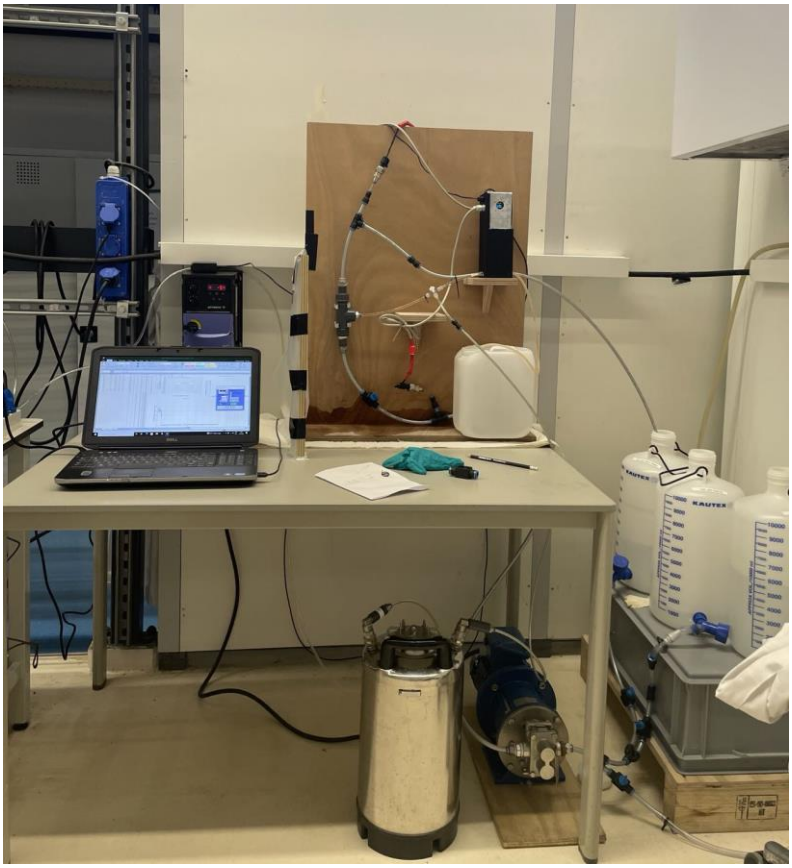

Figure 12 The picture of experimental setup

In this research, fouling tests were done on both coated and pristine ceramic membranes using SA model solution and surface water. 31 mg/L of SA solution was used in the filtration cycles under constant flux of around 170 L/(m^2·h), which is a common filtration flux for industry application of ultrafiltration membrane, and around 65 L/(m^2·h), which is lower but more friendly flux for nanofiltration membrane. The whole experiment consists of four different processes: 1) water permeability test with demi water, 2) fouling test with SA solution, 3) backwash with demi water and 4) chemical cleaning with NaClO solution. The water permeability of the membrane was tested first, followed by several cycles of fouling test, which lasted for 1 – 2 hours, and the backwash process, which lasts for 5 minutes. When the backwash efficiency was high enough for the membrane, another two cycles of fouling tests would be done. Finally the membrane was chemically cleaned with NaClO solution by soaking method. During the filtration cycles or chemical cleaning process, the feed solution in the 10 L jar tank was pumped into the membrane under a constant flux mode and the valve before the concentrate beaker was closed. When the valve was almost fully closed, one cycle of fouling experiment ended. The backwash system was linked to a compressed air vessel, which provided air pressure to press the demi water from the vessel through the permeate

side into the membrane. The backwash was done at the end of every cycle and the NaClO cleaning was done after one or three cycles of experiments to fully recovery its water permeability.

3.8 Backwash and fouling resistance

The backwash pressure was determined by the TMP at the end of the fouling cycle. Since the advised backwash flux is 2 to 3 times of the operational flux, the applied backwash pressure should be 2 to 3 times of the TMP when the fouling experiment was finished as derived in the equation below[18].

$$BWP = \frac{J_{BW}}{P_e} = \frac{a*J}{P_e} = a * TMP_e \qquad \textit{Equation 6}$$

Where BWP [bar] stands for backwash pressure; J_{BW} [LMH] means the backwash flux; a is the factor for the backwash flux, which has a value range from 2 – 3; P_e and TMP_e are the water permeability and transmembrane pressure at the end of the fouling cycle. The applied backwash flux in this research was 2 times of the operational flux for normal flux filtration tests and 3 times of the operational flux for lower flux filtration tests, so factor a was 2 or 3.

The recovery and efficiency η of backwash were calculated form the equation below:

$$Recovery = \frac{P_r}{P_o} \qquad \textit{Equation 7}$$

$$\eta = \frac{P_r - P_e}{P_o - P_e} \qquad \textit{Equation 8}$$

Where P_o [LMH/bar] stands for original water permeability, P_r [LMH/bar] means recovered water permeability and P_e [LMH/bar] for the water permeability at the end of current cycle.

Total fouling resistance R_t [m^{-1}] can be defined by the equation below[8, 89-91]:

$$R_t = \frac{TMP}{\mu*J} = R_m + R_r + R_{ir} \qquad \textit{Equation 9}$$

The R_m [m^{-1}] represents the intrinsic membrane resistance, which can be calculated from the TMP when only demi water is filtered. R_r [m^{-1}] is the reversible fouling resistance and this can be calculated from the TMP decrease due to the backwash. R_{ir} [m^{-1}] means the irreversible fouling resistance and it shows the fouling that cannot be removed by the backwash. This can be calculated by subtracting R_m and R_r from R_t.

4 Results and discussion

4.1 Characterization of solution

4.1.1 pH and conductivity measurement

As shown in Table 4, the used demineralized water to make all kinds of solution had a pH value around 5.8. Two different concentrations of NaClO solution used for chemical stability test had a high pH of over 12.

Table 4 pH and conductivity value of the solution used for experiments

Solution types	pH	Conductivity [uS/cm]
Demi water	5.968±0.067	0.8±0
1% NaClO solution	12.115±0.01	$34.1\pm0 \cdot 10^3$
5% NaClO solution	12.454±0.003	$131\pm0 \cdot 10^3$
31 mg/L of SA soltuion	6.732±0.051	10.1±0
31 mg/L of SA solution with 0.5 mM Ca^{2+}	6.414±0.022	118.3±0
31 mg/L of SA solution with 2 mM Ca^{2+}	6.398±0.028	446.7±0.5
Surface water after 5 microns cartridge filtration	7.270±0.021	980.7±2.4

As elucidated in the equations below, NaClO first forms Na^+ and ClO^-. The ClO^- tends to combine the H^+ and produce HClO (hypochlorous acid), leaving less H^+ and more OH^- in the solution. This results in the high pH in the NaClO solution. With higher concentrations of NaClO, more protons are combined so the pH value is higher as well.

$$NaClO \leftrightarrow Na^+ + ClO^-$$

$$ClO^- + H_2O \leftrightarrow HClO + OH^-$$

For the foulant solution used in the fouling experiments, the addition of sodium alginate into the demi water increased the pH from 5.9 to 6.7 since the alginate anions tend to combines the H^+ as well, leading to an increase in pH value. The dosing of $CaCl_2$ into the solution reduces the solution pH because the Ca^{2+} has higher affinity to alginate anions and this results in the release of protons.

4.1.2 Size distribution of foulant solution

The particle size distribution of the foulant solution was measured by the Zetasizer Nano ZS (Malvern Panalytical) using dynamic light scattering (DLS). The concentration of foulant solution for fouling test (based on 31 mg/L SA) was too low to get valid results from the machine. Therefore, the concentration of tested SA solution was tenfold the original one to maintain good PDS quality. The results of the PSD by intensity of 300 mg/L SA solution with the addition of 0.5 and 2 mmol/L of Ca^{2+} are shown in Figure 13, Figure 14 and Figure 15. As can be obviously observed, there are two peaks occurring for each type of foulant solution and the dominant peak has larger average particle size. With the addition of the Ca^{2+}, both peaks shift leftwards, which meant their average sizes became smaller. The dominant peak reduced from 336 nm to 238 nm and finally 171 nm. This phenomena was also observed in other literatures and explanation provided is that: the added Ca^{2+} balances the negative charges along the SA chains and crosslinks the SA molecules, forming compacted cross-linking clusters[92]; Ca^{2+} has larger chargers compared with Na^{+}, which induced less intermolecular repulsion, decreased swelling of the polymers and the sizes[93].

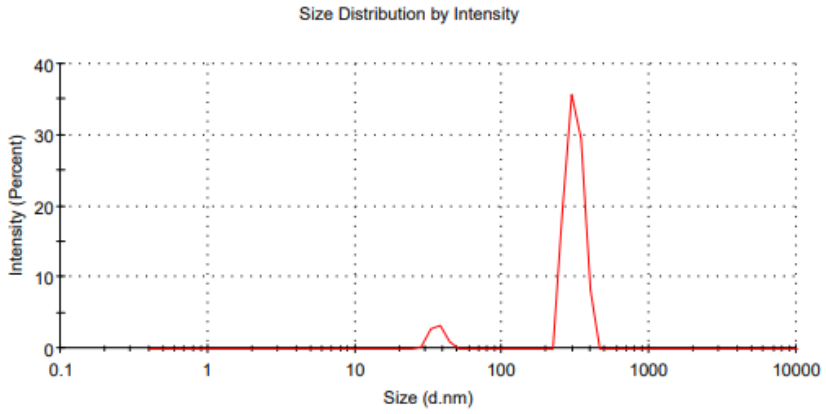

Figure 13 size distribution of 300 mg/L sodium alginate solution

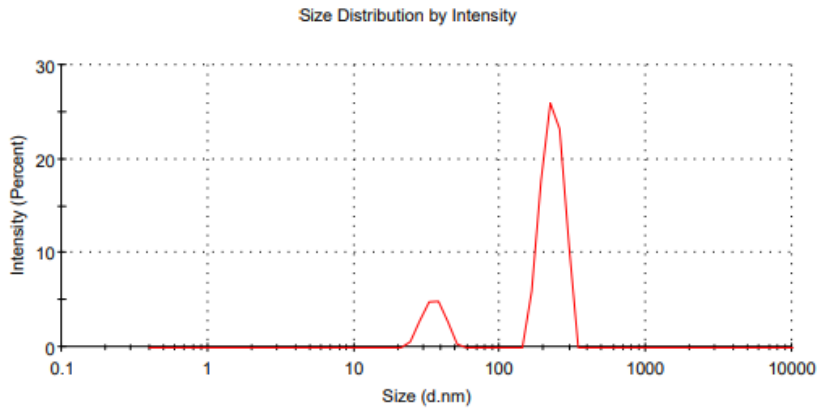

Figure 14 size distribution of 300 mg/L sodium alginate solution with 0.5 mmol/L of Ca^{2+}

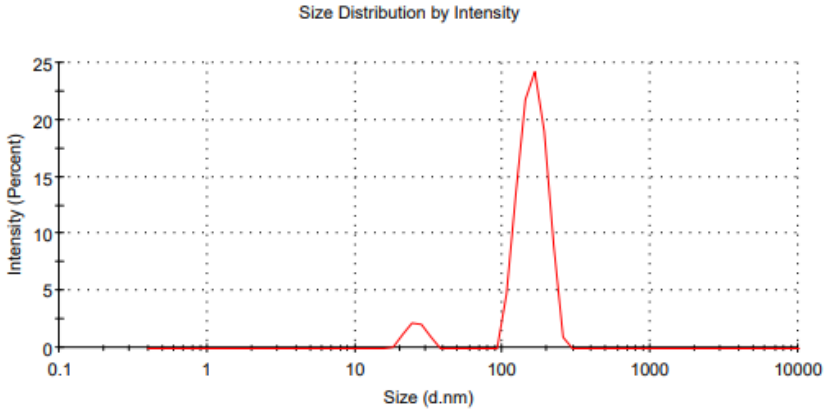

Figure 15 size distribution of 300 mg/L sodium alginate solution with 2 mmol/L of Ca^{2+}

4.1.3 Zetapotential of foulant solution

The zetapotential of foulant solution was also measured by Zetasizer Nano ZS (Malvern Panalytical). As can be seen from Figure 16, the 31 mg/L SA solution has the lowest value (-32.6 mV), which means it shows the strongest polyanionic character. The SA solution with 0.5 (-21.3 mV) and 2 mmol/L (-21.1 mV) of Ca has much smaller negative value, but the value difference between solution with 0.5 and 2 mmol/L of Ca^{2+} is very small. This indicates that the addition of Ca^{2+} has strong effect on reducing the negative charge at first due to the crosslink of Ca^{2+} to the negative site of alginates to form an 'egg box' as mentioned in 2.2.2. When the pH was near neutral, deprotonated carboxylic groups in the sodium alginates brought high negative charges, and this charges were neutralized by the addition of Ca^{2+}, which preferentially binded the carboxylic groups in good order[21]. But after a certain amount, the addition of Ca^{2+} has gradually less influence on the charge of the solution. This was probably due to

the limited carboxylic groups for binding. The surface water has the lowest negative zetapotential (-13.6 mV) among four types of solution. This is mainly due to the presence of other natural organic matters like humic acids and fulvic acids.

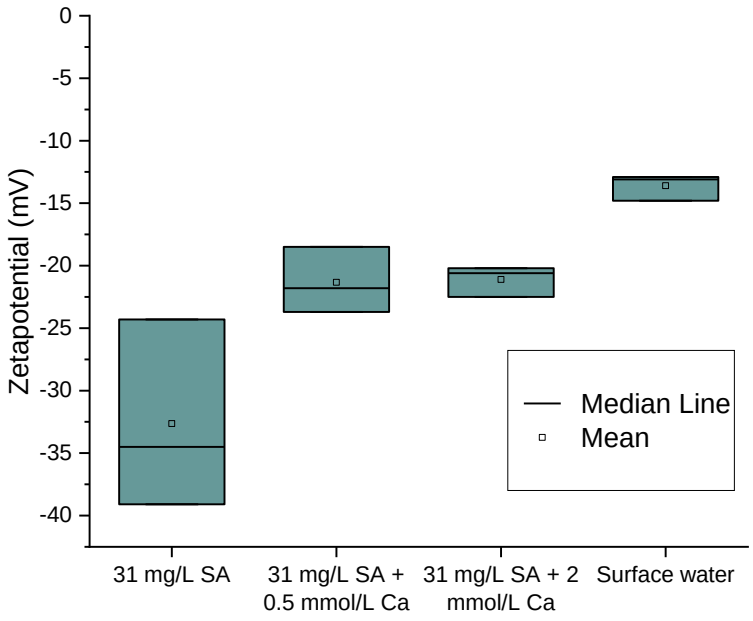

Figure 16 Zetapotential of four different types of foulant solution

4.2 Chemical stability test

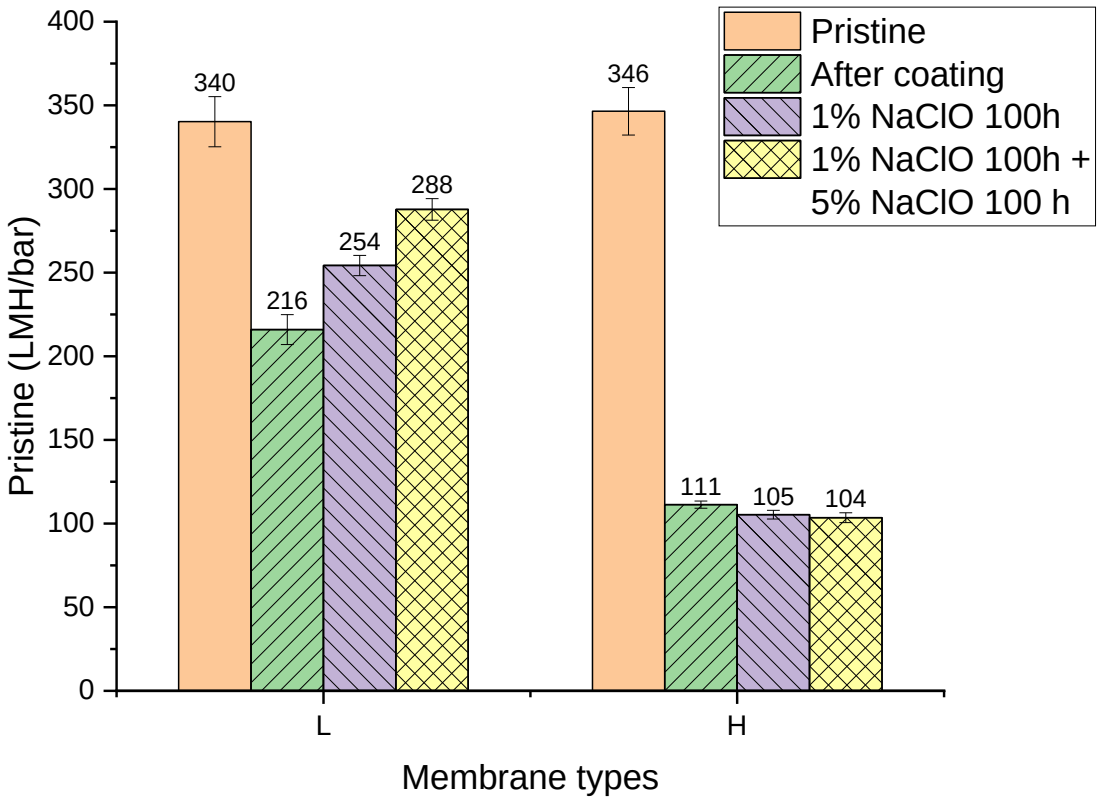

Figure 17 Water permeability change after NaClO soaking

According to Figure 17, the water permeability for the pristine membrane of L (coated under 750 °C for 60 minutes) and H (coated under 860 °C for 30 minutes) are both around 340 LMH/bar. After coating, the permeabilities drop to 216 LMH/bar and 111 LMH/bar for membrane L and H respectively. First both membranes were soaked in 1% of NaClO solution for 100 hours and then in 5% of NaClO solution for another 100 hours.

For membrane L, the permeability increased by 30.6% and then another 27.4% after two periods of soaking, accompanied by the colour change of membrane L and the NaClO solution surrounding it. The membrane L used to be grey, but during the soaking process it gradually lost its grey colour and the original white colour from alumina appeared. The colour of the surrounding NaClO solution changes from almost no colour to yellow during both period of experiments. This indicates a strong corrosion on the SiC layer coated under 750 °C: the layer gets corroded and dissolved into the solution, resulting in the colour vanishment on the membrane and the deepening of the solution colour. During the experiment process, the corrosion of SiC layer which has smaller pore size than pristine alumina membrane leads to the

increase of the water permeability. Therefore, no further fouling experiments under lower flux were done on membrane L.

For membrane H, the permeability only shows negative change within 5.4%, which is within the accuracy of the permeability measurement during the filtration test. The colour of membrane H and the solution surrounding it showed almost no changes: no apparent colour fading was observed on the brown membrane H, and the NaClO solution remained transparent for 1 % and a bit bright yellow for 5 % solution. The results of permeability change reveal an excellent chemical stability in relatively high concentration of NaClO solution for membrane H while an apparent corrosion in even lower concentrations of NaClO solution for membrane L. It means the membrane coated under 860 °C is more stable in NaClO solution than membrane coated under 750 °C.

SiC is a kind of ceramic material which has high resistance to oxidation. When fabricated with temperature below 850°C, amorphous SiC films would be synthesized[94]. Therefore, the SiC on membrane L and membrane H were both amorphous SiC. Due to the coating under relative high temperature, a thin SiO_2 layer was found to present on top of the SiC layer[95]. A literature showed that the solubility of SiO_2 increased dramatically when the pH of the solution exceeded 9[96]. However, this still cannot explain the dissolution of the SiC layer on membrane L to the NaClO solution. With the increase of fabrication temperature, less distortion of Si-C bonds was observed, which means the amorphous SiC becomes more stable[97]. However, no study was found to show the influence of bond distortion on its oxidation resistance. Therefore, the question why membrane coated under different temperatures showed different stability in NaClO solution remained unsolved in this research as it was beyond the scope of this thesis.

4.3 Carmen-Kozeny model estimation

After the substitution of the parameters in the assumptions, the Carmen-Kozeny equation was written as:

$$P_w = \frac{J}{TMP} = \frac{\varepsilon^{1.5} D^2}{32 \mu l} \qquad \textit{Equation 10}$$

As can be seen, the water permeability P_w is exponentially related to the pore size and porosity. First by substituting the permeability of the pristine membrane P_w (346 LMH/bar or $9.49 \cdot 10^{-10}$ m/(Pa·s)), its selective layer thickness l ($2.67 \cdot 10^{-5}$ m, which was measured from

SEM image of membrane L after 200 h of soaking in NaClO solution as shown in Figure 27), viscosity μ (0.001 Pa·s) and pore size D ($7.1 \cdot 10^{-8}$ m) , the membrane porosity ε was calculated to be 0.29.

According to the assumption, the overall porosity didn't change after coating. Therefore, by applying the measured permeability of membrane L and membrane H (233.5 LMH/bar and 111 LMH/bar or $6.4 \cdot 10^{-10}$ m/(Pa·s) and $3.04 \cdot 10^{-10}$ m/(Pa·s)), the estimated pore size of membrane L and membrane H were 58 nm and 40 nm. In Chen et al.'s paper, the pore size of same type of membrane as membrane L was measured to be 55 nm by capillary flow porometry, which was quite close to the estimated value in this research [8]. Therefore, the estimated pore size of membrane H was trustworthy.

4.4 Fouling experiments

4.4.1 Influence of calcium under normal flux for artificial solution

As can be seen from Figure 18, when the filtration was done using 31 mg/L SA solution, membrane H showed a good antifouling character, with much slower decrease of permeability and increase in pressure than membrane P and membrane L. The fouling time for membrane H of the first cycle lasted longer than 10 hours, which is more than four times longer than the first cycle of membrane L and P. The fouling mechanism can be easily recognized to be cake filtration as the main part of the pressure curve shows a linear increase. This is probably due to the sufficient electrostatic force between foulant solution and membrane material. Both the foulant solution and selective layer of membrane H are negatively charged. The electrostatic force between them is determined by the charge value according to Coulomb's Law. Membrane H had the largest negative charge among all three types of membranes. The performance during the first cycle of membrane L was better than the membrane P; but for the second and third cycle, the membrane L fouled quicker than membrane P.

At the beginning of each curve, a quick decrease of water permeability can be observed. For membrane H, L and P the extents were around 10%, 20% and 25% respectively. Similar phenomena was reported for SA filtration with Except from the fluctuation of pressure caused by switching the feed solution from demi water to foulant solution, another reason for this can be the different electrostatic forces between the membrane surface and the foulant solution. Membrane H was coated under higher temperature the largest negative charge, followed by membrane L and membrane P. When the repulsion force is strong enough, it takes less time to form the cake filtration mode. However, for membrane P the zetapotential at pH around

6.7 is smaller than membrane L (-15 mV for membrane P and -27 mV for membrane L according to [11]), resulting in larger extent of decrease during stabilization period.

Another phenomenon observed on this curve is that there exists an sharper decrease of permeability at the end of each cycle. This can be explained by the decrease of cross-flow velocity. Since in this experiment, the constant flux mode was maintained by only one pump and a valve.. When fouling happened on the membrane, higher TMP was required to produce permeate under constant flux. By closing the valve on the recirculating tube, TMP was increase, while the cross-flow velocity was decreased and finally approach 0 (valve completely closed to achieve higher TMP). A lower cross-flow velocity led to the loss of shear force, a force that contributed largely to the removal of SA layer from the membrane surface[19]. When less foulant was removed, a sharp decrease of permeability and increase of pressure happened. This phenomenon should be avoided during the practical operation because it makes the filtration process less effective with a large amount of fouling formed within a very short time.

When another 0.5 mmol/L of Ca^{2+} was added into solution, all types of membrane showed a rapid fouling within 20 minutes and no linear increase of pressure, which corresponds to cake filtration mode according to the fouling model mentioned before, was observed. At the pH of around 6.4, membrane P and membrane L should has the zetapotential around -10 mV and -25mV [11]. Since the zetapotential of foulant solution increased from -32.6 mV to -21.3 mV after the addition of Ca^{2+}, the electrostatic interaction between selective layer and foulant solution was weakened. What's more, the combination of Ca^{2+} and SA was proved to enhance the SA interactions between each other and this can lead to the subsequently deposition of SA foulant[12]. Another explanation for the quick fouling can be attributed to the quicker formation of gel layer after the addition of Ca^{2+}[14]. The solution in gel layer had lower chemical potential compared with the area above the gel layer and below the gel layer. Therefore, a potential gap needed to be fulfilled by offering extra pressure[98], causing heavier fouling. Even though the membrane H still had stronger repulsion force than membrane P, its fouling performance was the worst. This can be explained by that: the operational flux exceeded the critical flux for membrane H since the pressure increased in an exponential trend, just like the TMP curve operated under super-critical flux condition in Miller et al.'s research[65]. Even though membrane L and membrane H should have similar repulsion force against foulants, smaller pore size of membrane H than other membranes could increase the local flux to above the operational flux, causing larger drag force towards the membrane thus increasing

fouling[99, 100]. What's more, the higher TMP caused by the smaller pore size of membranes under constant flux mode tends to create more fouling, especially at the early stage of the filtration[101]. For membrane P, the fouling of all three cycles were almost the same. However, for membrane L, it got fouled more heavily in the subsequent cycle even though it performs better than membrane P in the first cycle. The change of the fouling behaviours after cycles can be attributed to the decrease in cross-flow velocity at the start of each cycle. Since the pump power stayed the same among three cycles, the closing extents of the valve were different to guarantee the same flux. Lower cross-flow velocity results in more rapid gathering of foulant on top of the membrane surfaces. As the increase of inlet pressure, more complete blocking might happen, which contribute to the fouling of membrane L. Another explanation can be that due to the decrease of surface roughness after a round of backwash, alginate was prone to attach to smoother surfaces and that results in more rapid fouling in the next filtration cycle[70, 71].

When more Ca^{2+} was dosed into the solution, both the pH value and zetapotential of foulant solution didn't show much change. The zetapotential of all membranes remained almost the same as well. However, the fouling curve revealed different fouling behaviours. The membrane L showed best antifouling performance, followed by membrane P and membrane H. For membrane H, the current flux was still beyond the critical flux as the pressure was still increasing exponentially[65]. The cause of worse performance of membrane P than membrane L could be the electrostatic force: the electrostatic force between the foulant solution and membrane P was smaller than that of membrane L.

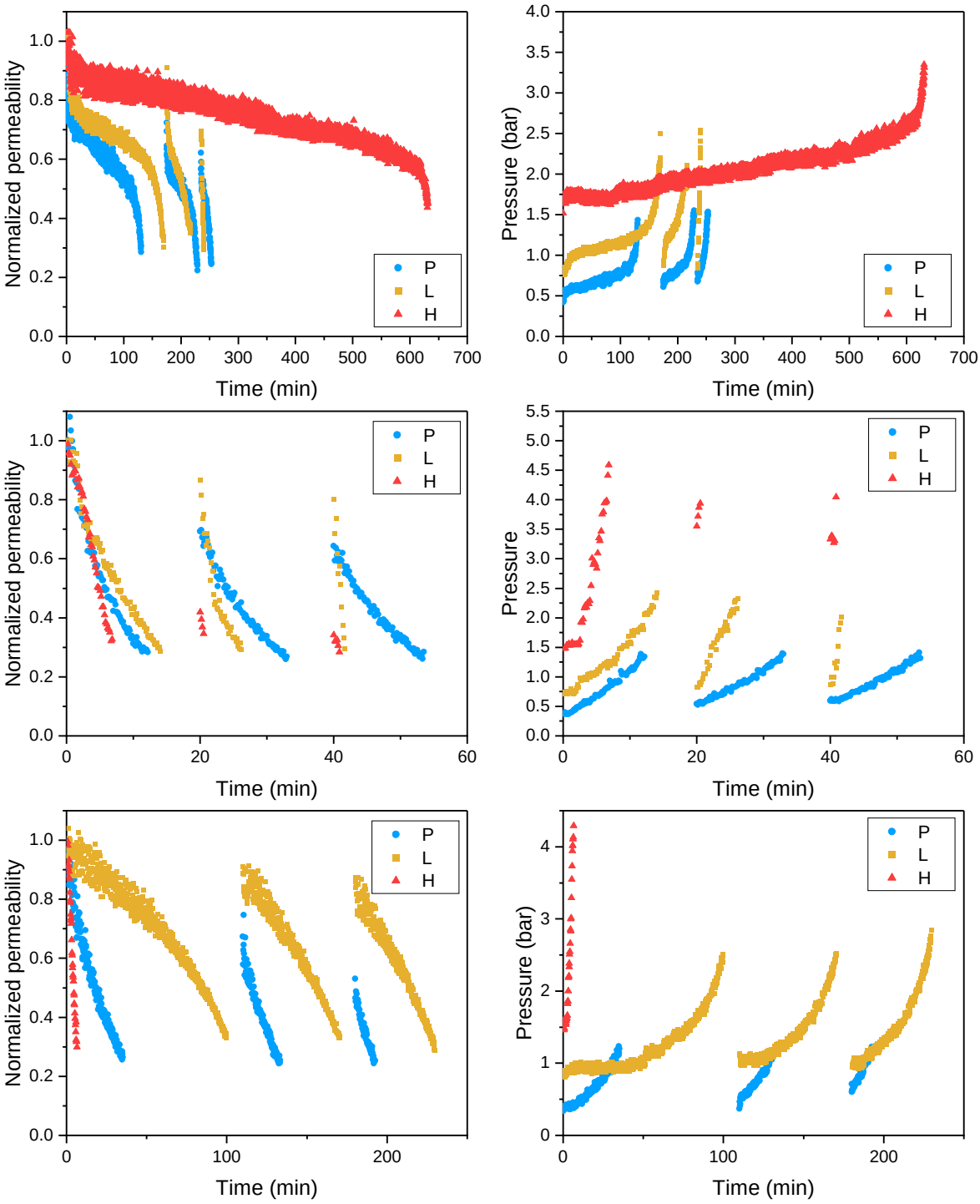

Figure 18 The normalized permeability and pressure to time curve of membrane P (the pristine membrane), L (coated membrane under 750 °C for 60 min) and H (coated membrane under 860 °C for 30 min) when filtrating 31 mg/L SA (up), 31 mg/L SA with 0.5 mmol/L Ca^{2+} (middle) and 31 mg/L SA with 2 mmol/L Ca^{2+} (bottom) solution under normal flux around 170 LMH

4.4.2 Influence of flux for artificial water

Since the normal flux (around 170 LMH), applied in the fouling experiment, apparently exceeded the critical flux of the membrane H, a lower flux (around 65 LMH) was applied for filtration test, using 31 mg/L of SA solution with 2 mmol/L Ca^{2+}. Because the transport of the foulants during normal flux was almost three times higher than during lower flux, the permeate volume during the fouling test was used as x-axis to evaluate the influence of the lower flux accurately apart from the lower cake layer build up brought by lower foulant transport speed. As can be seen from Figure 19, a lower flux did not alleviate the fouling process of the membrane H, the normalized permeability curves almost overlapped each other. Only slight changes in the slope could be observed. The pressure curves of the membrane H still showed exponential increases, which could mean the lower flux was still above the critical flux. A possible explanation could be the bridging effect of Ca^{2+} between alginates and membrane surface, which were both negatively charged[16, 17]. However, for membrane P, a lower flux changed the increase of pressure from exponential to linear, which indicates the mechanism of cake filtration[64]. Similar changes of fouling mechanism brought by lowering flux were found by other researches as well, who emphasized the importance of operating below critical flux[15, 65, 76].

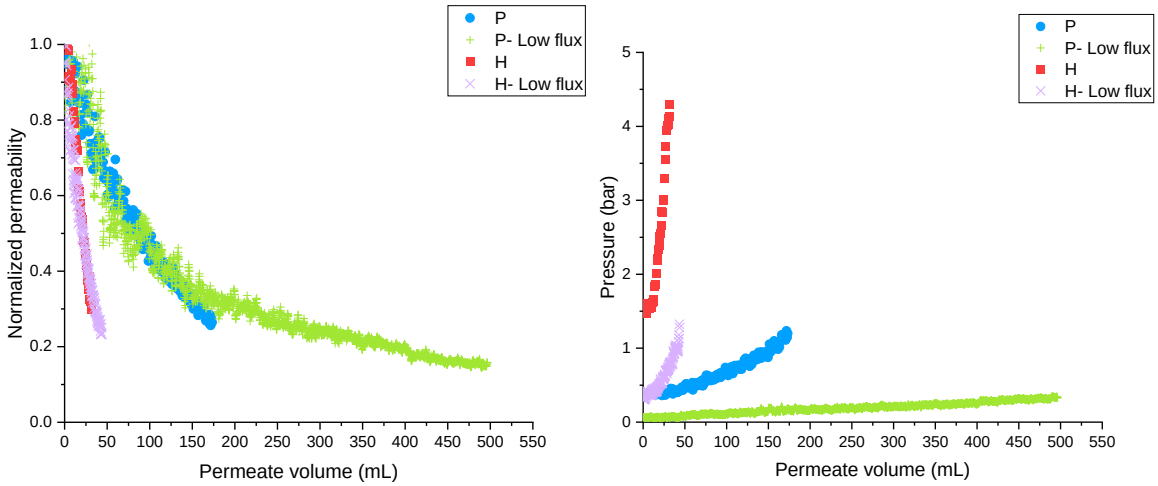

Figure 19 The normalized permeability and pressure to time curve of membrane P and membrane H under flux of 170 LMH and 65 LMH using 31 mg/L SA with 2 mmol/L Ca^{2+} as foulant solution

4.4.3 Influence of flux during filtration of surface water

For the surface water after filtration over a 5 micron's cartridge filter, membrane P, under both fluxes, showed a cake filtrate mode[64]. The decrease of flux only influenced the linear slope of TMP for membrane P. For membrane H, the lower flux was apparently under critical flux. The pressure curve of membrane P changed from exponential increase to linear increase, which means the fouling mechanism changed to cake filtration[64]. This could be explained by that higher TMP and higher local flux enhanced the convective deposition, resulting in larger dragging force on foulants than the lift force provided by electrostatic repulsion between foulants and membrane surface[102]. When comparing membrane P and membrane H, data shown that membrane H had almost the same fouling trend as membrane P with two differences. One is that it took membrane H shorter time to stabilize and this was probably still due to the stronger electrostatic repulsion force between membrane H and foulant solution than the repulsion force between foulant solution and membrane P: according to the data mentioned before, the zetapotential of membrane P was -15 mV, while for membrane H, its zetapotential should be around -27 mV, which was around the zetapotential of β-SiC under pH of 6.7[11, 38]. Thus more adsorption happened for membrane P in the first stage, causing lager extent of decrease in permeability[15]. After the membrane was already covered with a layer of negatively charged foulant, interactions between foulants took place and reduced the fouling trend. This was called the 'loading effect' mentioned by van der Brink who did SA fouling test on polycarbonate membranes[15]. Another difference is that membrane P had smaller fouling time of the first cycle, which was caused by the limitation of the experiment setup. If there were two pumps working at the same time, the fouling cycle of the membrane P can be more complete.

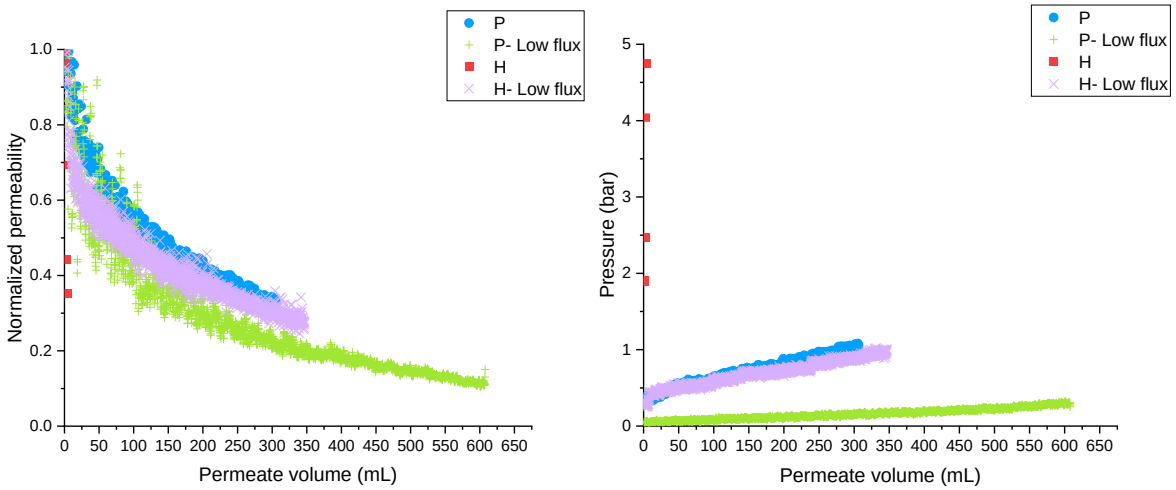

Figure 20 The normalized permeability and pressure to time curve of membrane P and membrane H under flux of 170 LMH and 65 LMH using surface water after 5 micron's cartridge filter

4.5 Backwash and fouling resistance analysis

4.5.1 Backwash recovery and efficiency comparison

The backwash fluxes used for membranes fouled under normal flux conditions in each cycle were between 307 to 378 LMH, which were around 2 times of the operational flux (170 LMH). For membranes fouled under lower flux conditions, the applied backwash fluxes were between 191 to 210 LMH, which were around 3 times of the operational flux (65 LMH). The detailed backwash fluxes on each fouling experiments were shown in Table 6 in the Appendix.

Among the three types of membranes, presented in Figure 21 and Figure 22, only membrane P was able to be backwashed during the fouling experiments under normal flux (170 LMH) with all four types of foulant solution. However, the overall recovery of membrane P was between 53% to 75%, which was lower than that of membrane L (between 75% to 88%). The backwash efficiency η gave the same trend: the overall efficiency of membrane P (52% to 88%) was lower than that of membrane L (76% to 94%). This data was comparable to that of Chang et al. (2015), who achieved 56% of hydraulic cleaning efficiency with demineralized water[74]. The backwash of membrane H was only successfully for 31 mg/L SA solution with 0.5 mmol/L Ca^{2+} and the recovery was lower than 33% in two rounds of backwash, which indicates inefficiency. With the addition of Ca^{2+}, both recovery and efficiency of the second backwash for membrane L gradually increased, while for membrane P, the recovery decreased and the efficiency fluctuated. This means that the addition of Ca^{2+} favours the

backwash of membrane L more than that of membrane P. This was probably due to the electrostatic repulsion forces between the foulant solution and the selective layer of membrane L, even though the coating of membrane L was not so stable as mentioned in 4.2.

Another noticeable difference in efficiency was that almost all the efficiency of the second backwash was higher than that of the first backwash. This was probably caused by the relatively longer fouling time during the first cycle, compared to the second cycle, and the fixed backwash time. Due to the limitations in the setup, the cycle always ended in a certain TMP range for different membranes: i.e. in each cycle the fouling curve ended at around 2.5 bar for membrane L when filtering 31 mg/L of SA solution with 2 mmol/L of Ca^{2+}. This means the P_e for a membrane was almost the same. However, the first fouling cycle had a larger P_o and resulted in larger denominator in the efficiency equation.

For the recovery and efficiency data during the lower flux experiments, two types of membranes (membrane P and H) and two types of foulant solution (31 mg/L SA + 2 mmol/L Ca^{2+} and surface water) were used. Only membrane P was successfully backwashed when filtering foulant solution with 2 mmol/L of Ca^{2+}. Both values were low in the 1^{st} and 2^{nd} backwash. It indicated that efficient backwash was more easily achieved under higher operational pressure than under a lower operational pressure. The longer fouling time in one cycle under lower flux made the backwash less efficient as well.

Overall, the backwash flux applied in all these experiments was insufficient to remove the gel layer (optical observation in 4.5.2) even though the backwash fluxes were 2 times and 3 times of the operational fluxes for experiments done under normal and lower flux. This was probably due to the inefficient backwash pressure and the strong bridging effect between the foulants and the membrane material[16, 17]. Therefore, the conclusion about the efficiency of the backwash was not possible.

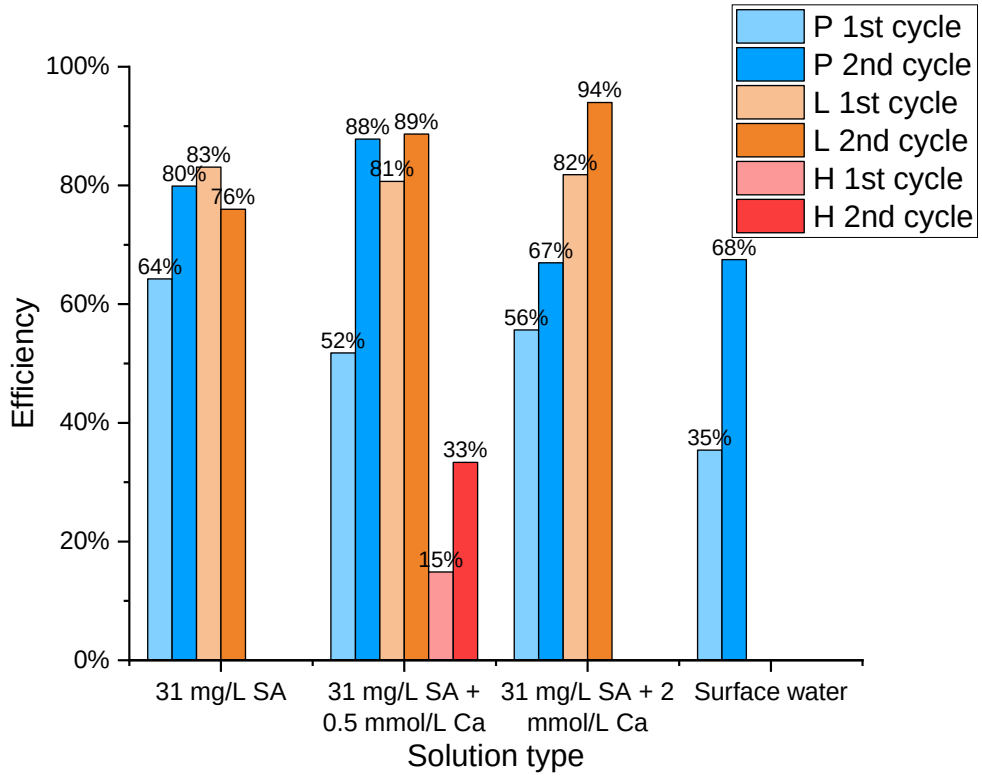

Figure 21 The backwash recovery of membranes fouled under normal flux (170 LMH) with backwash flux from 344 to 375 LMH

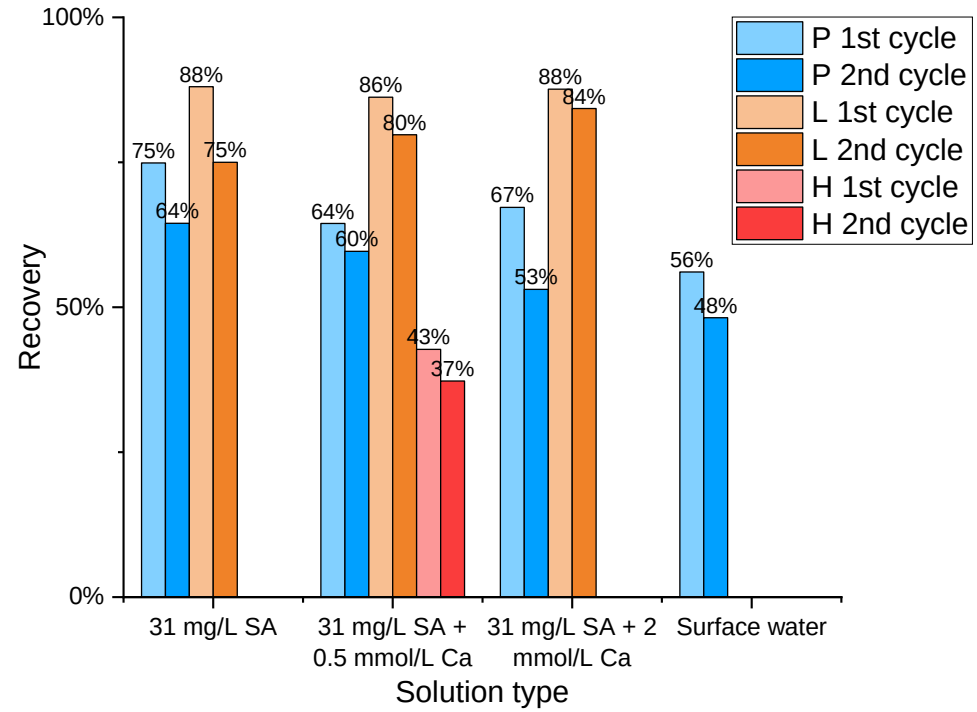

Figure 22 The backwash efficiency of membranes fouled under normal flux (170 LMH) with backwash flux from 344 to 375 LMH

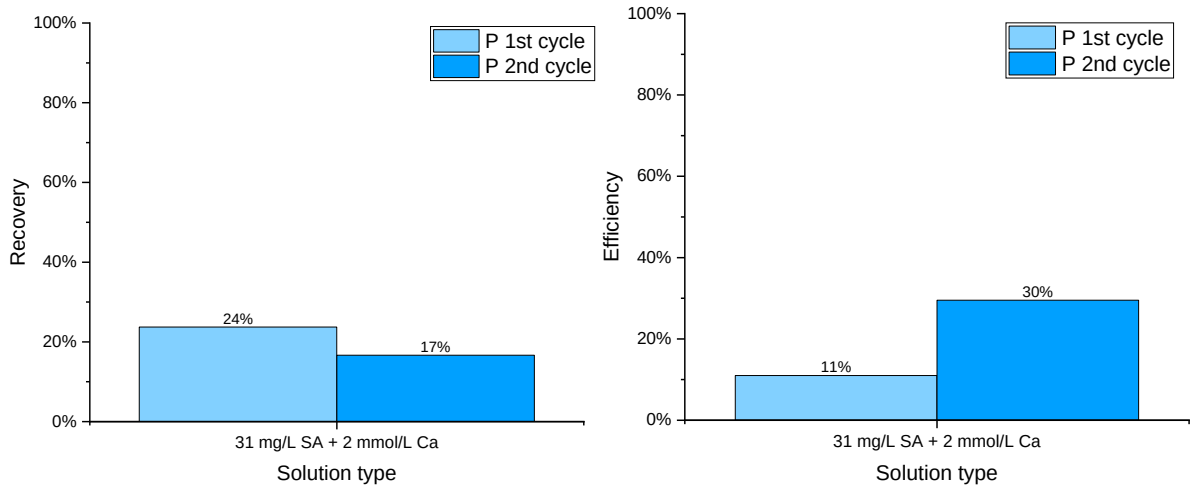

Figure 23 The backwash recovery (left) and efficiency (right of membrane P fouled under lower flux (65 LMH) with backwash flux of 191 LMH

4.5.2 Gel layer image

Occasionally, a complete foulant layer on top of the membrane was washed out when the backwash started (Figure 24). It happened only when abackwash pressure of 6 bar and backwash flux around 680 LMH (doubled the backwash pressure of 3 bar and backwash flux of 344 LMH during the fouling test) were applied on membrane P. No gel layer was observed to be washed out for membrane L or H because the backwash flux was much lower. From the images it can be observed that a large amount of small pores can be found on in the almost transparent gel layer. These pores were made during the backwash flux of around 680 LMH. An efficient backwash should remove a complete gel layer, which would guarantee a good performance in the next fouling cycle. However, for the fouling experiments presented in this thesis, no gel layer was observed to be washed out among three cycles even though the recovery for some cases was quite high. This means the backwash only flushed out smaller pores on the gel layerduring the backwash period instead of removing the whole gel layer into the concentrate. The gel layer formed during the filtration was still sticked to the membrane surface. This was also the finding by Shal et al. (2018) who observed that a biofouling layer was only partially released during the backwash with pure water[103]. When the next fouling cycle began, new fouling settled on top of the old fouling layer.

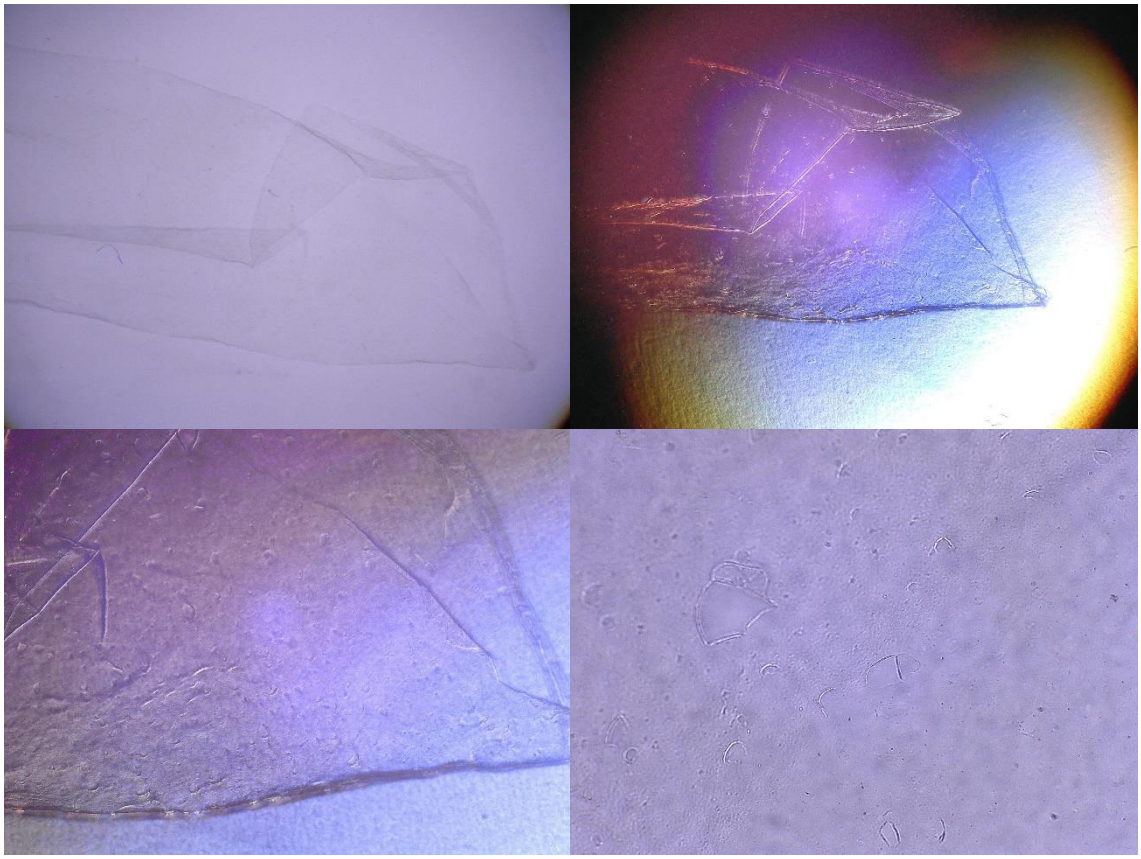

Figure 24 The images of gel layer washed out from membrane P when backwash pressure of 6 bar and backwash flux of around 680 LMH was applied (up left: 20X; up right: 20X; bottom left: 40X; bottom right: 80X)

4.5.3 Fouling resistance comparison

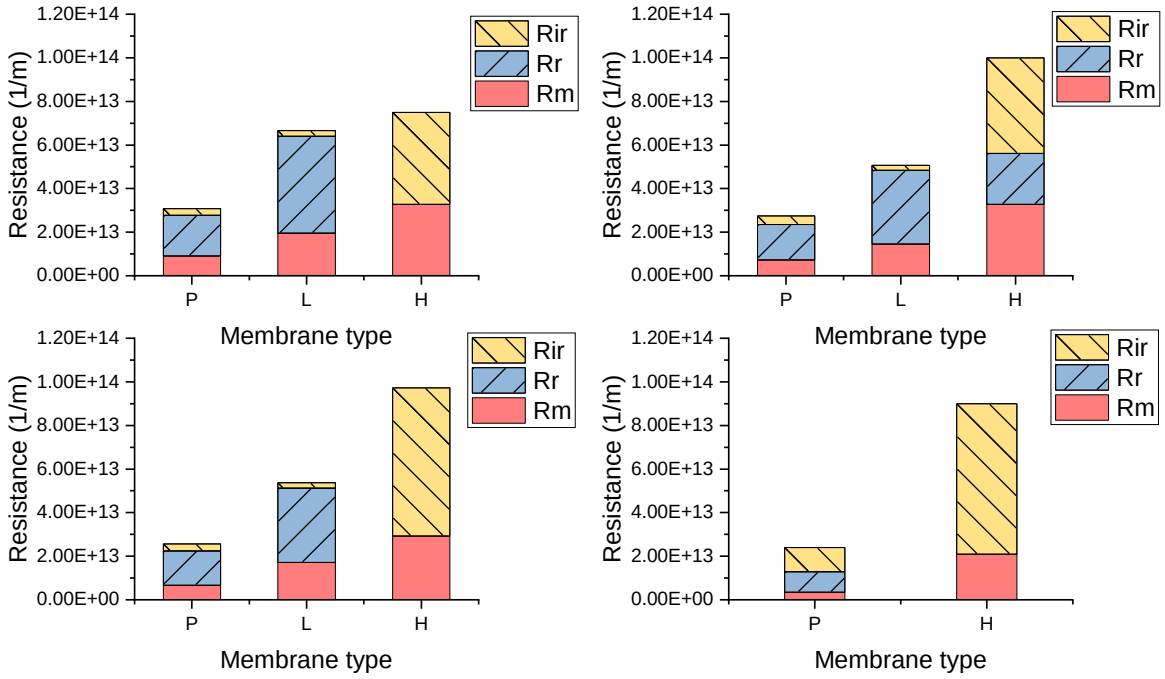

Figure 25 Fouling resistance of different types of membrane for the 1st cycle when filtering 31 mg/L SA (up left), 31 mg/L SA with 0.5 mmol/L Ca^{2+} (up right), 31 mg/L SA with 2 mmol/L Ca^{2+} (bottom left) solution under normal flux around 170 LMH and 31 mg/L SA with 2 mmol/L Ca^{2+} (bottom right) solution under lower flux around 65 LMH

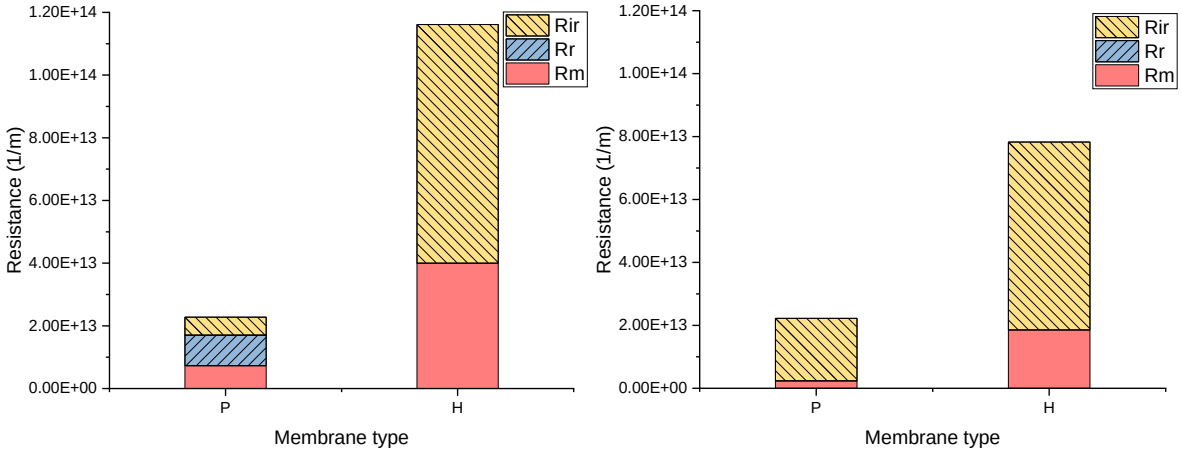

Figure 26 Fouling resistance of different types of membrane for the 1st cycle when filtering surface water under normal flux around 170 LMH (left) and under lower flux around 65 LMH (right)

Since the backwash was inefficient for all the fouling experiments, the fouling resistance calculated based on that could be inaccurate. The fouling resistance includes intrinsic membrane resistance R_m, reversible resistance R_r and irreversible resistance R_{ir}. The R_r was calculated from the difference between the recovered permeance and the clean water permeance. Therefore, when the backwash failed to remove all the hydraulic reversible fouling, the calculated R_r could be smaller than the real one. In some experiments, no recovery of water permeability was observed after the backwash. In this case, the calculated R_r was 0, and the total fouling resistance was made up of R_m, which was calculated from the clean water permeability, and R_{ir}, which was calculated from subtracting R_m from the total fouling calculated from the water permeability at the end of each fouling cycle. The detailed formula was mentioned in 3.8.

As can be observed from Figure 25, the R_m increased with the decrease of pore size for membrane P (71 nm), L (55 nm) and H (40 nm). This is due to the fact that resistance is inverse proportional to the water permeability, and the water permeability increases as the pore size increases according to the Hagen–Poiseuille equation[104]. For membrane H, most of the fouling was irreversible under this backwash condition. The reversible fouling only occurred during the filtration of SA solution with 0.5 mmol/L of Ca^{2+}, this was probably because membrane H had the smallest fouling time when filtering this foulant solution compared with other foulant solutions (7 min compared with 10 h and 30 min). This finding was consistent with the finding by Munla et al. (2012) who observed that irreversible fouling is characterized by much slower flux decline while reversible fouling by quicker flux decline for constant pressure filtration [102]. More reversible fouling and less irreversible fouling were found on membrane P and L, which means that these two membranes functioned well under the given operational parameters. For surface water, fouling besides polysaccharides existed (humic acids, bacteria and other ions) and this made the demineralized water backwash efficiency lower. However, when the flux was decreased, the irreversible resistance for membrane P increased.

Another finding related to the irreversible fouling resistance is that this parameter showed a linear increase according to time. The addition of Ca^{2+} increased the magnitude of the accumulation of irreversible fouling resistance per minute ΔR_{ir} and then decrease for membrane P and membrane L. This find was consistent with the unimodal pattern of gel layer resistance with the increase in Ca^{2+} concentration by Zhang et al.[14].

Table 5 The linear regression of the membrane irreversible resistance according to time

	Membrane type	R0 [1/m]	ΔR_{ir} [1/(m·min)]	R^2
31 mg/L SA	P	9E12	3E10	0.9878
	L	2E13	3E10	0.8151
31 mg/L SA + 0.5	P	8E12	2E11	0.8708
mmol/L Ca^{2+}	L	1E13	2E11	0.9947
	H	3E13	1E13	0.9779
31 mg/L SA + 2	P	7E12	1E11	0.9968
mmol/L Ca^{2+}	L	2E13	2E11	0.9953
(Lower flux)	P	4E12	3E10	0.9857
Surface water	P	7E12	9E10	0.9998

5 Conclusions, limitations and recommendations

5.1 Conclusions

In this study, chemical stability tests and fouling experiments were done on two types of SiC-Al_2O_3 ultrafiltration membrane fabricated using LPCVD method under different coating temperature. After coating, SiC-Al_2O_3 membrane coated under a higher temperature (membrane H) only had half the pure water permeability of the low temperature coated membrane (membrane L).

a) **Chemical stability of SiC coated membrane in NaClO solution**

   Membrane H showed a good chemical stability in a NaClO solution, with almost no change on the water permeability after 200 h of soaking experiment. However, membrane L was not stable in the NaClO solution, showing an increase in water permeability and the dissolution of the coating layer after 200 h of experiment.

b) **Fouling features of SiC coated membrane compared with pristine Al_2O_3 membrane**

   Membrane H also had a better antifouling ability compared with membrane L and the pristine alumina membrane (membrane P), when filtering SA solution and the surface water, which both had negative zetapotential. The electrostatic interactions between membrane surface and the foulant solution were assumed to largely contribute to the antifouling ability of the coated membrane when its force was not overcome by the super-critical flux. Cake filtration, which indicated an good fouling performance, was observed when the operational flux was lower than the critical flux.

c) **Backwash analysis on coated and pristine membrane**

   The backwash flux applied in all the experiments was insufficient to remove the gel layer on the fouled membranes, resulting in an inefficient cleaning efficiency. However, a gel layer removal was observed when backwash flux that was four times of the operational flux was applied, which implied the necessity of increasing backwash pressure.

d) **The influence of calcium on the fouling and backwash**

   The addition of Ca^{2+} reduced the fouling performance of coated membrane first due to the decrease of electrostatic interactions and then the quick adsorption of foulant particles to the membrane surface in the early stage by bridging effect. The addition of

Ca^{2+} had limited influence on the backwash recovery and efficiency of membrane P after the addition of Ca^{2+} while slight improvement was observed for membrane L.

e) The influence of flux reduction on the fouling and backwash

The reduction of the operational flux obviously improved the fouling performance of membrane H when filtering surface water, which was probably related to the sub-critical flux operation. Membrane H had a low critical flux compared with membrane P and membrane L, while it changed with different types of foulant solution. For a pure SA solution, the normal flux (170 LMH) was already below the critical flux, while for SA solution with Ca^{2+} the lower flux (65 LMH) was still too high. Therefore, little effect was observed on the fouling using SA solution with more Ca^{2+}. However, this lower flux was below the critical flux for membrane H when filtering surface water. The change of fouling mechanism to cake filtration indicated a stronger effect of electrostatic forces than inlet pressure for membrane H under a lower flux. The backwash efficiency and recovery both decreased after the decrease of operational flux, which indicates that more fouling were irreversible under lower flux.

5.2 Limitations

This research was done under the constant flux mode without circulation pump. A valve was used to increase the pressure at the outside part of the membrane so that the constant permeated flux was guaranteed. This resulted in the changing of crossflow velocity, which is another important factor that effects the membrane fouling due to the shear force it provided. When the valve was almost fully closed, the crossflow velocity became small and the shear force was too weak to maintain a stable fouling. This limited the fouling capacity of a membrane at even though it did save the energy cost of the circulation pump.

During the foulant solution characterisation part, Zetasizer Nano ZS was unable to detect a valid particle size distribution of the foulant solution used in the research. Therefore, a larger concentration of the SA solution was used to obtain a valid data. This could lead to a deviation of the particle size when it was used to compare with the pore size of the membrane during the fouling mechanism analysis.

The Carman-Kozeny model was used to estimate the pore size of the coated membrane. However, this model was used to estimate the pressure drop for laminar flow through a packed bed solids. In our case, the water used for pure water permeability test was turbulent flow and the ceramic membrane was not a perfect packed bed. Several assumptions were made in this model. These might cause deviation between the estimated pore size and the real one even though the result of one set of data was quite close to the estimated one.

The backwash was inefficient for the fouling experiments in this research. This resulted in the lack of data on reversible fouling resistance especially for the membrane H. Therefore, a small amount of the reversible fouling resistance might be neglected in the study.

5.3 Recommendations

a) Crossflow velocity control

Since the crossflow velocity was not formally recorded in this study, the addition of a flow meter at the circulation tube can be considered. This parameter should be controlled or studied in the future work to reveal its influence on the fouling of the coated membrane.

b) Improvement on characterizing the fouling

Better technique could be used to get better particle size distribution results of the foulant solution. More methods should be considered on the characterisation of the fouling layer before and after the backwash. The foulant mass balance can be done by analysing the concentrations of the foulant in the influent, permeate and the backwash concentrate to acquire the amount of the foulant particles in the fouling layer. Then the foulant rejection and the backwash efficiency on removing specific ions can be used for further evaluation on the membrane and backwash. Since only SA and surface water were tested in this research, more foulant like HA and BSA as well as their combinations could be considered for further analysis.

c) Further study on backwash

The complete gel layer washed out after hydraulic backwash indicated the high efficiency of reversible fouling removal under higher backwash pressure. Since this research focused mainly on the fouling study instead of systematic backwash study. Further study can be done on finding the optimal backwash pressure for the coated membrane.

d) Further study on chemical stability

No explanation was offered for the chemical stability difference between the low and high temperature coated membranes. Further study can be done on more literature reviewing and membrane characterisation about the difference of the SiC layer brought by coating temperature. What's more, this research only used NaClO solution for the chemical stability test. More cleaning solutions like NaOH and citric acid can be tested in the future.

6 References

1. Wada, Y., et al., *Modeling global water use for the 21st century: the Water Futures and Solutions (WFaS) initiative and its approaches.* Geosci. Model Dev., 2016. **9**(1): p. 175-222.
2. Komolafe, C., et al., *MODERN CONVENTIONAL WATER TREATMENT TECHNOLOGIES AND CHALLENGES FOR OPTIMAL UTILIZATION IN NIGERIA.* 2013.
3. Mika, S. and L. Irina, *Chapter 8 - Ion Exchange*, in *Natural Organic Matter in Water*. 2015. p. 239-273.
4. Kamali, M., et al., *Sustainability considerations in membrane-based technologies for industrial effluents treatment.* Chemical Engineering Journal, 2019. **368**: p. 474-494.
5. Asif, M.B. and Z. Zhang, *Ceramic membrane technology for water and wastewater treatment: a critical review of performance, full-scale applications, membrane fouling and prospects.* Chemical Engineering Journal, 2021: p. 129481.
6. König, K., et al., *One-step deposition of ultrafiltration SiC membranes on macroporous SiC supports.* Journal of Membrane Science, 2014. **472**: p. 232-240.
7. Nagano, T., K. Sato, and K. Kawahara, *Gas Permeation Property of Silicon Carbide Membranes Synthesized by Counter-Diffusion Chemical Vapor Deposition.* Membranes, 2020. **10**(1): p. 11.
8. Chen, M., et al., *Highly permeable silicon carbide-alumina ultrafiltration membranes for oil-in-water filtration produced with low-pressure chemical vapor deposition.* Separation and Purification Technology, 2020. **253**: p. 117496.
9. Wei, W., et al., *Preparation of non-oxide SiC membrane for gas purification by spray coating.* Journal of Membrane Science, 2017. **540**: p. 381-390.
10. De Lange, R., et al., *Formation and characterization of supported microporous ceramic membranes prepared by sol-gel modification techniques.* Journal of membrane science, 1995. **99**(1): p. 57-75.
11. Chen, M., et al., *Oil-in-water emulsion separation: Fouling of alumina membranes with and without a silicon carbide deposition in constant flux filtration mode.* Water Research, 2022. **216**: p. 118267.
12. Moyo, W., et al., *Fundamental fouling mechanisms of dissolved organic matter fractions and their implications on the surface modifications of ceramic nanofiltration membranes: insights from a laboratory scale application.* Water Science and Technology, 2019. **80**(9): p. 1702-1714.
13. De Angelis, L. and M.M.F. de Cortalezzi, *Ceramic membrane filtration of organic compounds: Effect of concentration, pH, and mixtures interactions on fouling.* Separation and Purification Technology, 2013. **118**: p. 762-775.
14. Zhang, M., et al., *Effect of calcium ions on fouling properties of alginate solution and its mechanisms.* Journal of membrane science, 2017. **525**: p. 320-329.
15. Van den Brink, P.F.H., *Gel layer formation on membranes in membrane bioreactors.* 2014.

16. Li, S., et al., *Fouling control mechanisms of demineralized water backwash: Reduction of charge screening and calcium bridging effects.* Water research, 2011. **45**(19): p. 6289-6300.
17. Li, S., et al., *Impact of backwash water composition on ultrafiltration fouling control.* Journal of Membrane Science, 2009. **344**(1-2): p. 17-25.
18. Hofs, B., et al., *Comparison of ceramic and polymeric membrane permeability and fouling using surface water.* Separation and Purification Technology, 2011. **79**(3): p. 365-374.
19. Arndt, F., et al., *Influence of operating parameters and membrane materials on fouling of ceramic hollow fibre membranes.* Separation and Purification Technology, 2016. **171**: p. 289-296.
20. Somiya, S. and Y. Inomata, *Silicon carbide ceramics. 1. Fundamental and solid reaction*. Vol. 13. 1991: Springer.
21. Katsoufidou, K., S.G. Yiantsios, and A.J. Karabelas, *Experimental study of ultrafiltration membrane fouling by sodium alginate and flux recovery by backwashing.* Journal of Membrane Science, 2007. **300**(1): p. 137-146.
22. Sondhi, R., R. Bhave, and G. Jung, *Applications and benefits of ceramic membranes.* Membrane Technology, 2003. **2003**(11): p. 5-8.
23. Das, D., et al., *Preparation and characterization of macroporous SiC ceramic membrane for treatment of waste water.* Journal of Porous Materials, 2018. **25**(4): p. 1183-1193.
24. Filtersafe. *HOW DOES FILTRATION PURIFY WATER: FILTRATION PROCESSES ACROSS THE SPECTRUM*. 2021 [cited 2022 13.08]; Available from: https://filtersafe.net/blog/blog-marine/how-does-filtration-purify-water-filtration-spectrum/.
25. Sonawane, S., et al., *Chapter 17 - Nanomaterials for membrane synthesis: Introduction, mechanism, and challenges for wastewater treatment*, in *Handbook of Nanomaterials for Wastewater Treatment*, B. Bhanvase, et al., Editors. 2021, Elsevier. p. 537-553.
26. Lee, M., Z. Wu, and K. Li, *2 - Advances in ceramic membranes for water treatment*, in *Advances in Membrane Technologies for Water Treatment*, A. Basile, A. Cassano, and N.K. Rastogi, Editors. 2015, Woodhead Publishing: Oxford. p. 43-82.
27. Qiu, M., et al., *1.11 Ceramic Membranes*, in *Comprehensive Membrane Science and Engineering (Second Edition)*, E. Drioli, L. Giorno, and E. Fontananova, Editors. 2017, Elsevier: Oxford. p. 270-297.
28. Xing, W.H., *Chapter 14 - Ceramic Membranes*, in *Membrane-Based Separations in Metallurgy*, L.Y. Jiang and N. Li, Editors. 2017, Elsevier: Amsterdam. p. 357-370.
29. Li, K., *Ceramic membranes for separation and reaction*. 2007: John Wiley & Sons.
30. Gitis, V. and G. Rothenberg, *Ceramic membranes: new opportunities and practical applications*. 2016: John Wiley & Sons.
31. Boffa, V. and E. Marino, *Inorganic materials for upcoming water purification membranes*, in *Current Trends and Future Developments on (Bio-) Membranes*. 2020, Elsevier. p. 117-140.

32. Ciora, R.J., et al., *Preparation and reactive applications of nanoporous silicon carbide membranes.* Chemical engineering science, 2004. **59**(22-23): p. 4957-4965.
33. Eom, J.-H. and Y.-W. Kim, *Effect of template size on microstructure and strength of porous silicon carbide ceramics.* Journal of the Ceramic Society of Japan, 2008. **116**(1358): p. 1159-1163.
34. Fraga, M., et al., *Morphological, chemical surface and filtration characterization of a new silicon carbide membrane.* Journal of the European Ceramic Society, 2017. **37**(3): p. 899-905.
35. Lee, L.L. and D.S. Tsai, *Silicon carbide membranes modified by chemical vapor deposition using species of low sticking coefficients in a silane/acetylene reaction system.* Journal of the American Ceramic Society, 1998. **81**(1): p. 159-165.
36. Labropoulos, A., et al., *Experimental investigation of the transport mechanism of several gases during the CVD post-treatment of nanoporous membranes.* Chemical Engineering Journal, 2014. **255**: p. 377-393.
37. Nguyen, T.-K., et al., *Superior Robust Ultrathin Single-Crystalline Silicon Carbide Membrane as a Versatile Platform for Biological Applications.* ACS Applied Materials & Interfaces, 2017. **9**(48): p. 41641-41647.
38. Nikkam, N., et al., *Fabrication, characterization and thermophysical property evaluation of SiC nanofluids for heat transfer applications.* Nano-Micro Letters, 2014. **6**(2): p. 178-189.
39. Reyes Bahena, J., et al., *Fluoride adsorption onto α-Al203 and its effect on the zeta potential at the alumina-aqueous electrolyte interface.* Separation Science and technology, 2002. **37**(8): p. 1973-1987.
40. Hermia, J., *Constant pressure blocking filtration laws: application to power-law non-Newtonian fluids.* Institution of chemical Engineers, 1982. **60**(3): p. 183-187.
41. Pereira, L. and J. Cotas, *Introductory chapter: Alginates-A general overview.* Alginates-Recent Uses of This Natural Polymer, 2020.
42. Senturk Parreidt, T., K. Müller, and M. Schmid, *Alginate-based edible films and coatings for food packaging applications.* Foods, 2018. **7**(10): p. 170.
43. Sudha, P.N., *Industrial applications of marine biopolymers*. 2017, Boca Raton: CRC Press. 626.
44. Emmerichs, N., et al., *Interaction between alginates and manganese cations: identification of preferred cation binding sites.* International Journal of Biological Macromolecules, 2004. **34**(1): p. 73-79.
45. Yang, J.-S., Y.-J. Xie, and W. He, *Research progress on chemical modification of alginate: A review.* Carbohydrate polymers, 2011. **84**(1): p. 33-39.
46. *Alginates Handling/Processing*. 2015, Agricultural Marketing Service, US Department of Agriculture.
47. Draget, K.I., O. Smidsrød, and G. Skjåk-Bræk, *Alginates from algae.* Polysaccharides and polyamides in the food industry: properties, production, and patents, 2005: p. 1-30.
48. Donati, I. and S. Paoletti, *Material properties of alginates*, in *Alginates: biology and applications*. 2009, Springer. p. 1-53.

49. Andersen, T., P. Auk-Emblem, and M. Dornish, *3D Cell Culture in Alginate Hydrogels.* Microarrays, 2015. **4**(2): p. 133-161.
50. Haug, A., B. Larsen, and O. Smidsrød, *Uronic acid sequence in alginate from different sources.* Carbohydrate Research, 1974. **32**(2): p. 217-225.
51. Khanna, O., et al., *Synthesis of multilayered alginate microcapsules for the sustained release of fibroblast growth factor-1.* Journal of biomedical materials research Part A, 2010. **95**(2): p. 632-640.
52. Sarmento, B., et al., *Insulin-loaded nanoparticles are prepared by alginate ionotropic pre-gelation followed by chitosan polyelectrolyte complexation.* Journal of nanoscience and nanotechnology, 2007. **7**(8): p. 2833-2841.
53. Grant, G.T., *Biological interactions between polysaccharides and divalent cations: the egg-box model.* Febs Lett., 1973. **32**: p. 195-198.
54. Arunkumar, K., *Extraction, Isolation, and Characterization of Alginate*, in *Industrial Applications of Marine Biopolymers*, P.N. Sudha, Editor. 2017, CRC Press: Boca Raton. p. 19-35.
55. Papajová, E., et al., *Method for preparation of planar alginate hydrogels by external gelling using an aerosol of gelling solution.* Carbohydrate Polymers, 2012. **90**(1): p. 472-482.
56. Quong, D., et al., *External versus internal source of calcium during the gelation of alginate beads for DNA encapsulation.* Biotechnology and Bioengineering, 1998. **57**(4): p. 438-446.
57. Draget, K.I., K. Østgaard, and O. Smidsrød, *Homogeneous alginate gels: A technical approach.* Carbohydrate polymers, 1990. **14**(2): p. 159-178.
58. Chan, L.W., H.Y. Lee, and P.W.S. Heng, *Mechanisms of external and internal gelation and their impact on the functions of alginate as a coat and delivery system.* Carbohydrate Polymers, 2006. **63**(2): p. 176-187.
59. Flemming, H.-C. and J. Wingender, *The biofilm matrix.* Nature reviews microbiology, 2010. **8**(9): p. 623-633.
60. Katsoufidou, K., S. Yiantsios, and A. Karabelas, *Experimental study of ultrafiltration membrane fouling by sodium alginate and flux recovery by backwashing.* Journal of Membrane Science, 2007. **300**(1-2): p. 137-146.
61. Wu, D., J.A. Howell, and R.W. Field, *Critical flux measurement for model colloids.* Journal of Membrane Science, 1999. **152**(1): p. 89-98.
62. Cui, Z., et al., *Effect of Cross-flow Velocity on the Critical Flux of Ceramic Membrane Filtration as a Pre-treatment for Seawater Desalination.* Chinese Journal of Chemical Engineering, 2013. **21**(4): p. 341-347.
63. Field, R.W., et al., *Critical flux concept for microfiltration fouling.* Journal of Membrane Science, 1995. **100**(3): p. 259-272.
64. Kirschner, A.Y., et al., *Fouling mechanisms in constant flux crossflow ultrafiltration.* Journal of Membrane Science, 2019. **574**: p. 65-75.
65. Miller, D.J., et al., *Comparison of membrane fouling at constant flux and constant transmembrane pressure conditions.* Journal of Membrane Science, 2014. **454**: p. 505-515.
66. Kosmulski, M., *Compilation of PZC and IEP of sparingly soluble metal oxides and hydroxides from literature.* Advances in Colloid and Interface Science, 2009. **152**(1): p. 14-25.

67. Zhong, Z., et al., *Membrane surface roughness characterization and its influence on ultrafine particle adhesion.* Separation and Purification Technology, 2012. **90**: p. 140-146.
68. Zhong, Z., et al., *Adhesion of nanosized nickel catalysts in the nanocatalysis/UF system.* AIChE journal, 2007. **53**(5): p. 1204-1210.
69. Hashino, M., et al., *Effect of membrane surface morphology on membrane fouling with sodium alginate.* Journal of Membrane Science, 2011. **366**(1): p. 258-265.
70. Hashino, M., et al., *Effect of surface roughness of hollow fiber membranes with gear-shaped structure on membrane fouling by sodium alginate.* Journal of Membrane Science, 2011. **366**(1-2): p. 389-397.
71. Li, R., et al., *Effects of surface morphology on alginate adhesion: Molecular insights into membrane fouling based on XDLVO and DFT analysis.* Chemosphere, 2019. **233**: p. 373-380.
72. Verberk, J. and H. Van Dijk, *Research on AirFlush®: distribution of water and air in tubular and capillary membrane modules.* Water Science and Technology: Water Supply, 2003. **3**(5-6): p. 409-414.
73. Chang, H., et al., *Towards a better hydraulic cleaning strategy for ultrafiltration membrane fouling by humic acid: Effect of backwash water composition.* Journal of Environmental Sciences, 2016. **43**: p. 177-186.
74. Chang, H., et al., *Role of backwash water composition in alleviating ultrafiltration membrane fouling by sodium alginate and the effectiveness of salt backwashing.* Journal of Membrane Science, 2016. **499**: p. 429-441.
75. Kim, H.-G., et al., *Optimization of backflushing conditions for ceramic ultrafiltration membrane of disperse dye solutions.* Desalination, 2007. **202**(1): p. 150-155.
76. Ye, Y., et al., *Effects of operating conditions on submerged hollow fibre membrane systems used as pre-treatment for seawater reverse osmosis.* Journal of Membrane Science, 2010. **365**(1): p. 78-88.
77. Waterman, D.A., *Bench-scale analysis of ultrafiltration membranes for investigating fouling by natural organic matter in surface water*. 2008, University of Ottawa (Canada).
78. Ye, Y., V. Chen, and P. Le-Clech, *Evolution of fouling deposition and removal on hollow fibre membrane during filtration with periodical backwash.* Desalination, 2011. **283**: p. 198-205.
79. Hwang, K.-J., C.-S. Chan, and K.-L. Tung, *Effect of backwash on the performance of submerged membrane filtration.* Journal of Membrane Science, 2009. **330**(1): p. 349-356.
80. Whistler, R.L. and R. Schweiger, *Oxidation of Alginic Acid with Hypochlorite at Different Hydrogen Ion Concentrations1.* Journal of the American Chemical Society, 1958. **80**(21): p. 5701-5704.
81. Alresheedi, M.T., O.D. Basu, and B. Barbeau, *Chemical cleaning of ceramic ultrafiltration membranes - Ozone versus conventional cleaning chemicals.* Chemosphere, 2019. **226**: p. 668-677.
82. Chae, S.-R., et al., *Comparison of fouling characteristics of two different poly-vinylidene fluoride microfiltration membranes in a pilot-scale drinking water treatment system using pre-coagulation/sedimentation, sand filtration, and chlorination.* Water research, 2008. **42**(8-9): p. 2029-2042.

83. Tin, M.M.M., et al., *Membrane fouling, chemical cleaning and separation performance assessment of a chlorine-resistant nanofiltration membrane for water recycling applications.* Separation and Purification Technology, 2017. **189**: p. 170-175.
84. Yu, Z., et al., *Two-Dimensional FTIR Spectroscopic Characterization of Functional Groups of NaOCl-Exposed Alginate: Insights into Membrane Refouling after Online Chemical Cleaning.* ACS Applied Bio Materials, 2018. **1**.
85. Abdelrasoul, A., et al., *Mass transfer mechanisms and transport resistances in membrane separation process.* Mass Transfer-Advancement in Process Modelling, 2015: p. 15-40.
86. Seader, J., E.J. Henley, and D.K. Roper, *Separation process principles: With applications using process simulators*. 2016: John Wiley & Sons.
87. Kruczek, B., *Carman–Kozeny Equation*, in *Encyclopedia of Membranes*, E. Drioli and L. Giorno, Editors. 2015, Springer Berlin Heidelberg: Berlin, Heidelberg. p. 1-3.
88. Pisani, L., *Simple expression for the tortuosity of porous media.* Transport in Porous Media, 2011. **88**(2): p. 193-203.
89. Xing, J., et al., *Insight into Fe(II)/UV/chlorine pretreatment for reducing ultrafiltration (UF) membrane fouling: Effects of different natural organic fractions and comparison with coagulation.* Water Research, 2019. **167**: p. 115112.
90. Huang, B.-C., et al., *Membrane fouling characteristics and mitigation in a coagulation-assisted microfiltration process for municipal wastewater pretreatment.* Water Research, 2017. **123**: p. 216-223.
91. Rahimpour, A., et al., *Coupling TiO2 nanoparticles with UV irradiation for modification of polyethersulfone ultrafiltration membranes.* Journal of Membrane Science, 2008. **313**(1): p. 158-169.
92. El Nokab, M.E.H., et al., *Solid-state NMR spectroscopy insights for resolving different water pools in alginate hydrogels.* Food Hydrocolloids, 2022. **127**: p. 107500.
93. Shivakumara, L.R. and T. Demappa, *Synthesis and swelling behavior of sodium alginate/poly (vinyl alcohol) hydrogels.* Turkish Journal of Pharmaceutical Sciences, 2019. **16**(3): p. 252.
94. Bhaskaran, M., *Synthesis and characterization of LPCVD SiC films using novel precursors*. 1997: New Jersey Institute of Technology.
95. Qin, Y., et al., *Effect of deposition temperature on the corrosion behavior of CVD SiC coatings on SiCf/SiC composites under simulated PWR conditions.* Corrosion Science, 2021. **181**: p. 109233.
96. Krauskopf, K.B., *Dissolution and precipitation of silica at low temperatures.* Geochimica et Cosmochimica Acta, 1956. **10**(1): p. 1-26.
97. Foti, G., *Silicon carbide: from amorphous to crystalline material.* Applied Surface Science, 2001. **184**(1): p. 20-26.
98. Zhang, M., et al., *A new insight into membrane fouling mechanism in submerged membrane bioreactor: osmotic pressure during cake layer filtration.* Water research, 2013. **47**(8): p. 2777-2786.

99. Kasemset, S., et al., *Effect of polydopamine deposition conditions on polysulfone ultrafiltration membrane properties and threshold flux during oil/water emulsion filtration.* Polymer, 2016. **97**: p. 247-257.
100. Miller, D.J., et al., *Constant flux crossflow filtration evaluation of surface-modified fouling-resistant membranes.* Journal of Membrane Science, 2014. **452**: p. 171-183.
101. Kouchaki Shalmani, A., I.M.A. ElSherbiny, and S. Panglisch, *Application-oriented mini-plant experiments using non-conventional model foulants to evaluate new hollow fiber membrane materials.* Separation and Purification Technology, 2020. **251**: p. 117345.
102. Munla, L., S. Peldszus, and P.M. Huck, *Reversible and irreversible fouling of ultrafiltration ceramic membranes by model solutions.* Journal - American Water Works Association, 2012. **104**(10): p. E540-E554.
103. Shao, S., et al., *Biofouling in ultrafiltration process for drinking water treatment and its control by chlorinated-water and pure water backwashing.* Science of the total environment, 2018. **644**: p. 306-314.
104. Li, W., W. Xing, and N. Xu, *Modeling of relationship between water permeability and microstructure parameters of ceramic membranes.* Desalination, 2006. **192**(1): p. 340-345.

7 Appendix

7.1 The backwash fluxes applied on experiments

As can be seen in Table 6, the backwash fluxes and the backwash pressure applied on filtration tests were listed below. Since the operational flux was around 170 LMH for normal flux test and 65 LMH for lower flux test, the backwash flux doubled and tripled the operational flux of normal flux test and lower flux test respectively.

Table 6 The backwash fluxes applied on each experiments

	Membrane P		Membrane L		Membrane H	
	BW Pressure [bar]	BW flux [LMH]	BW Pressure [bar]	BW flux [LMH]	BW Pressure [bar]	BW flux [LMH]
31 mg/L SA solution	3	344	5	357	7	355
31 mg/L SA + 0.5 mmol/L Ca solution	3	378	5	378	8.5	357
31 mg/L SA + 2 mmol/L Ca solution	2.5	351	5	326	8.5	344
Surface water	2	318			8.5	307
31 mg/L SA + 2 mmol/L Ca solution lower flux	1	191			4	200
Surface water lower flux	1	210			3	195

7.2 The SEM image of membrane H

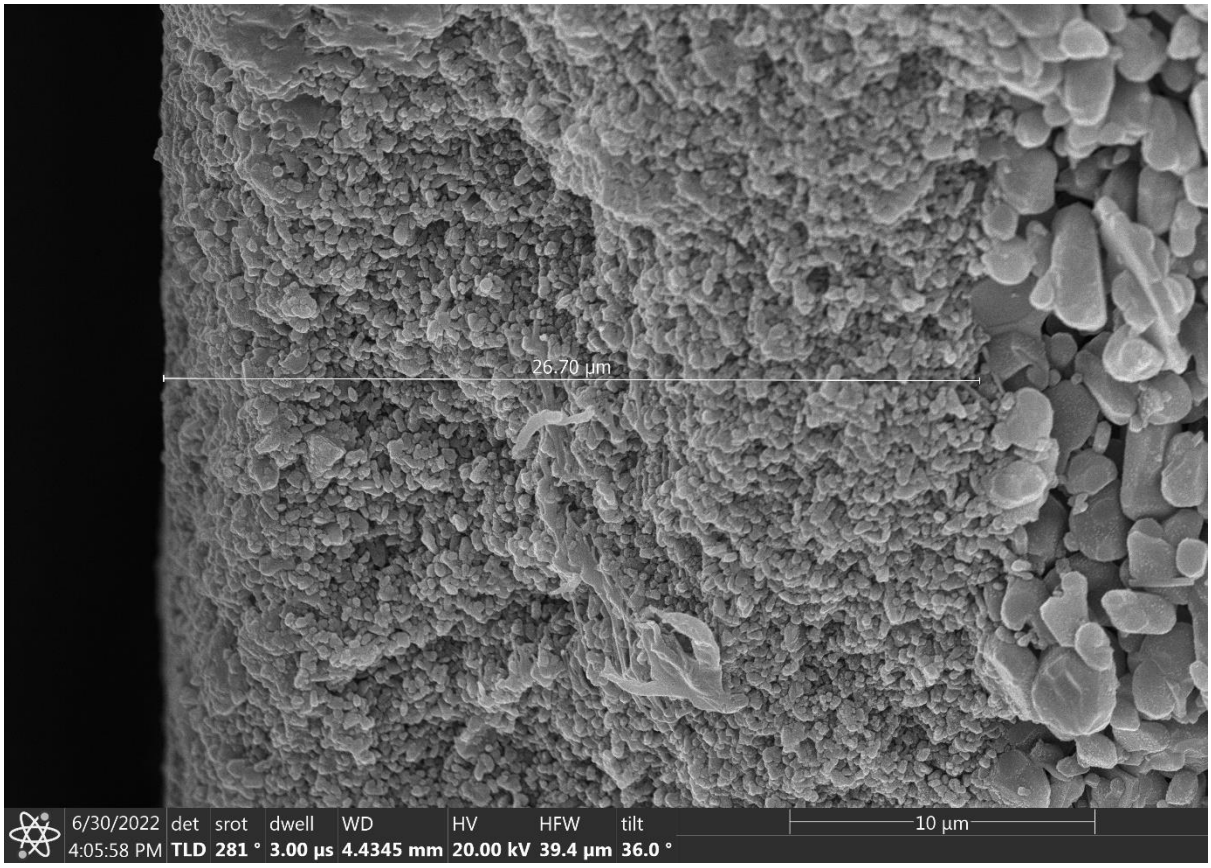

Figure 27 SEM image of membrane L after 200 h of soaking in NaClO solution

7.3 The fouling test for determining the used SA concentration under flux of 345 LMH

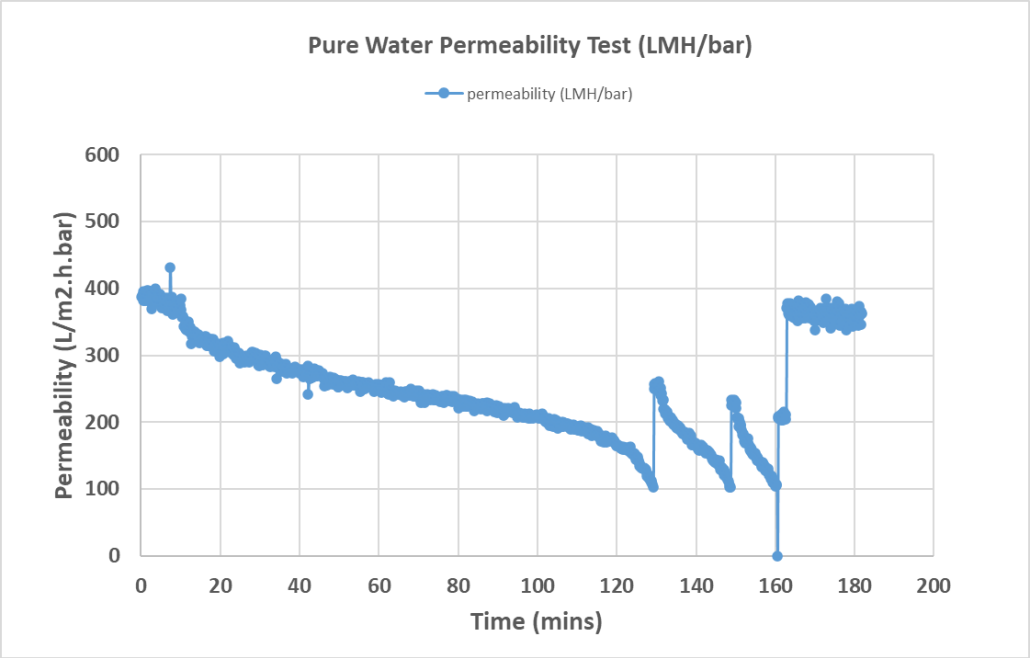

Figure 28 Membrane P filtering 7 mg/L SA solution with backwash pressure of 5 bar, duration of 5 minutes and final chemical cleaning with 0.5 % NaClO in ultrasound for 30 minutes

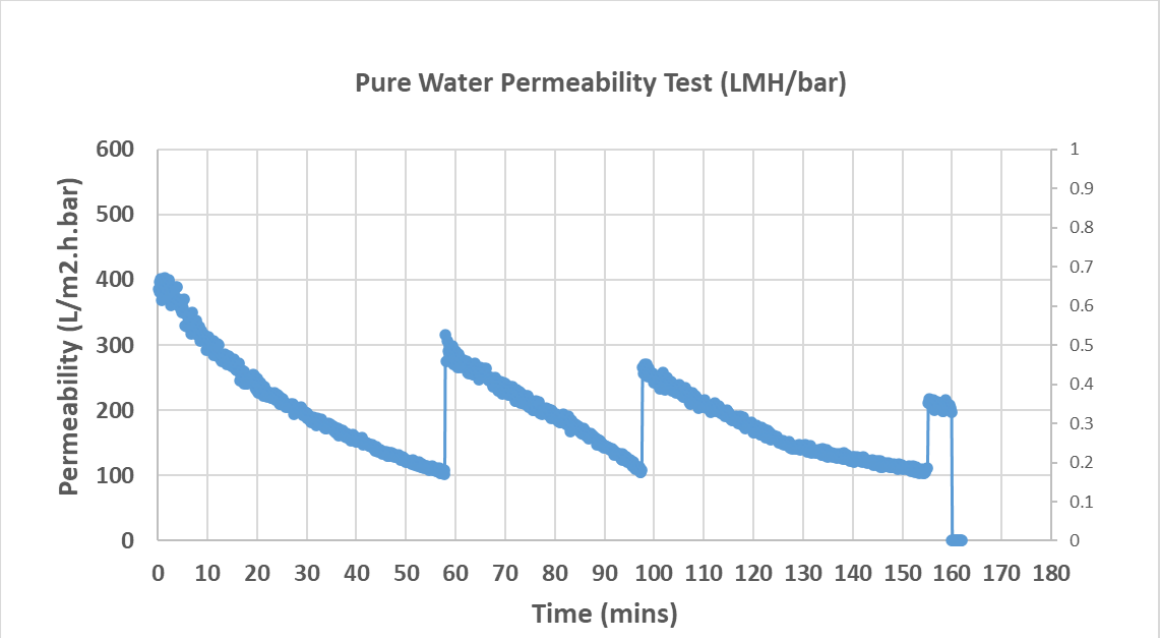

Figure 29 Membrane P filtering 7 mg/L SA solution with 2 mmol/L of Ca^{2+} with backwash pressure of 5 bar, duration of 5 minutes

7.4 The fouling test for determining the used SA concentration under flux of 170 LMH

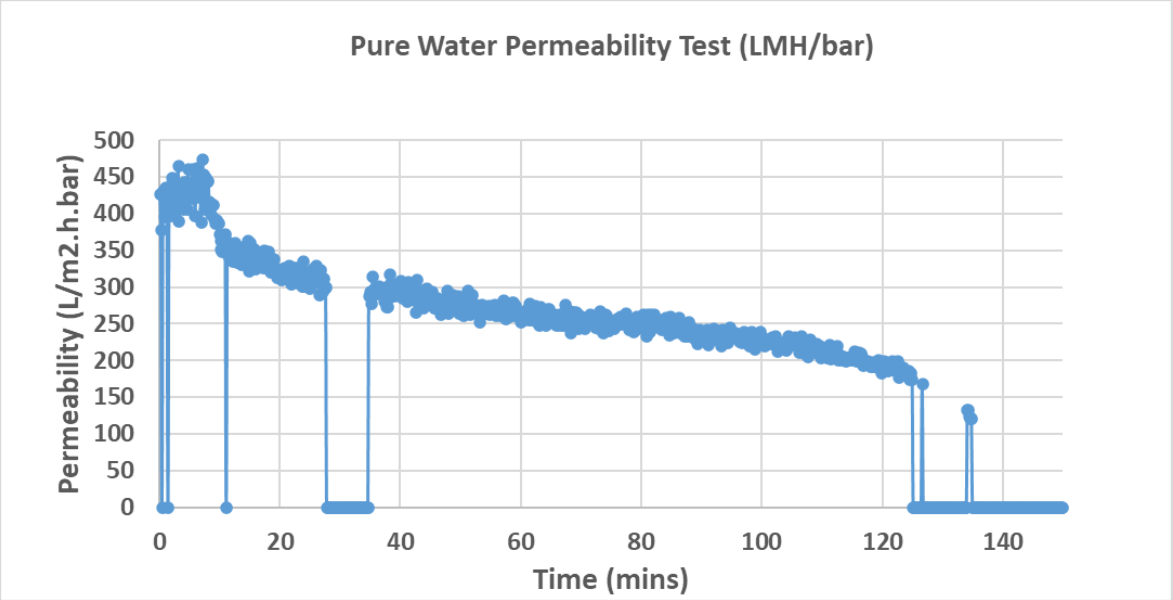

Figure 30 Membrane P filtering 30 mg/L SA solution

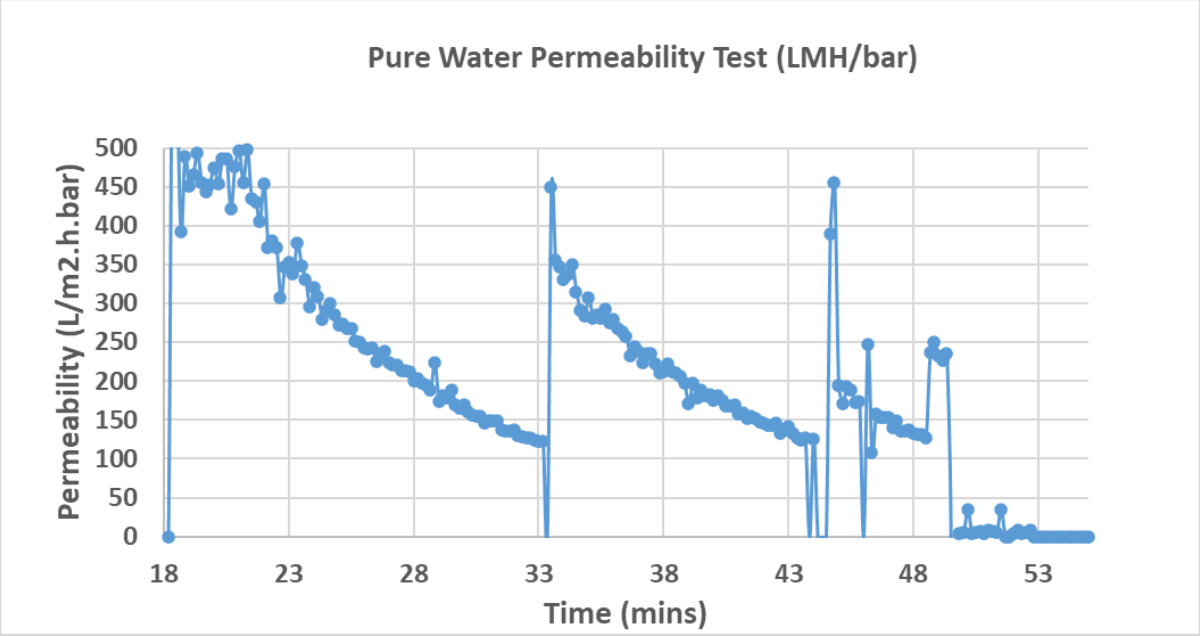

Figure 31 Membrane P filtering 30 mg/L SA solution with 0.5 mmol/L of Ca^{2+} with backwash pressure of 3 bar, duration of 5 minutes

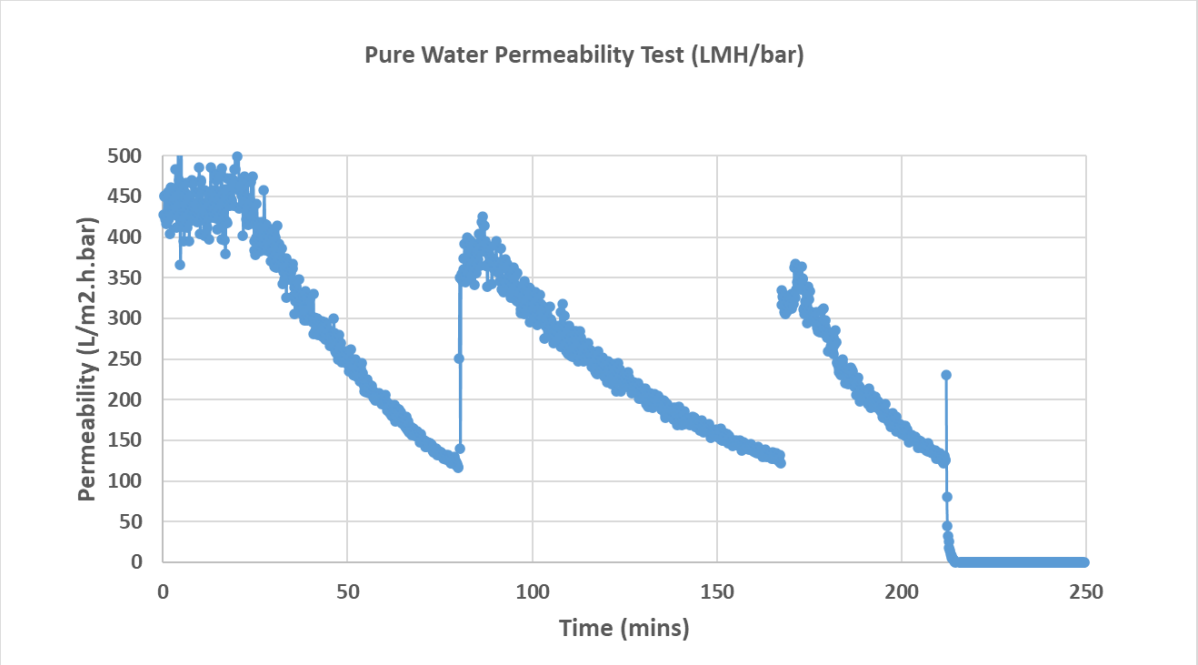

Figure 32 Membrane P filtering 10 mg/L SA solution with 0.5 mmol/L of Ca^{2+} with backwash pressure of 3 bar, duration of 5 minutes

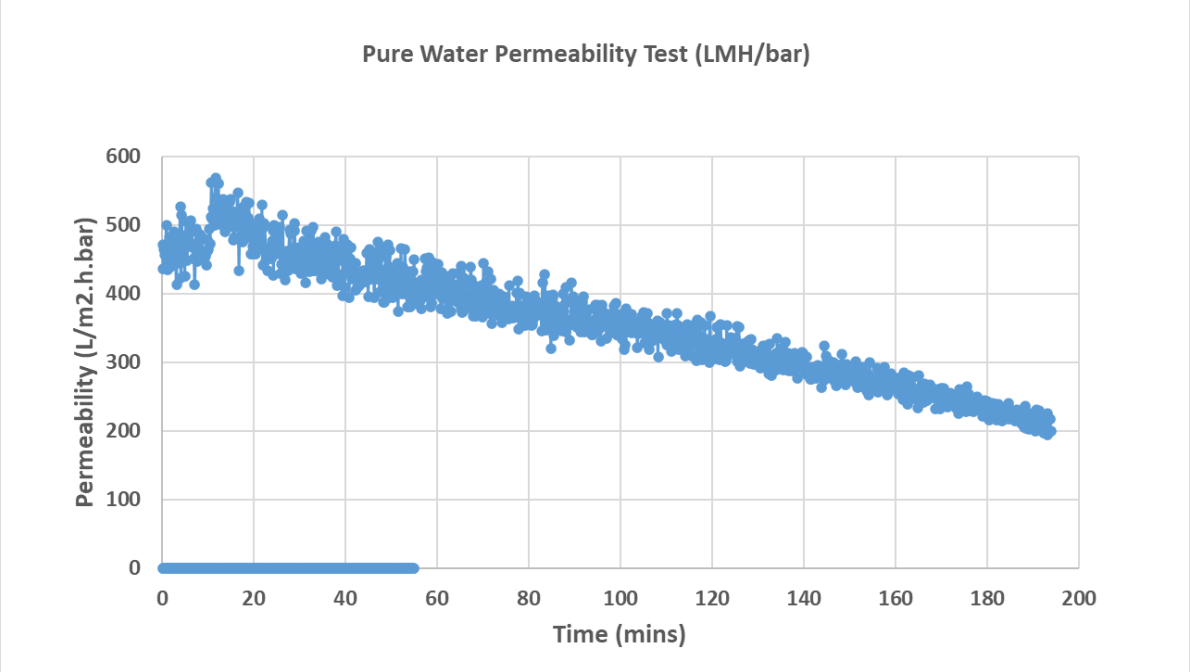

Figure 33 Membrane P filtering 10 mg/L SA solution with 2 mmol/L of Ca^{2+}

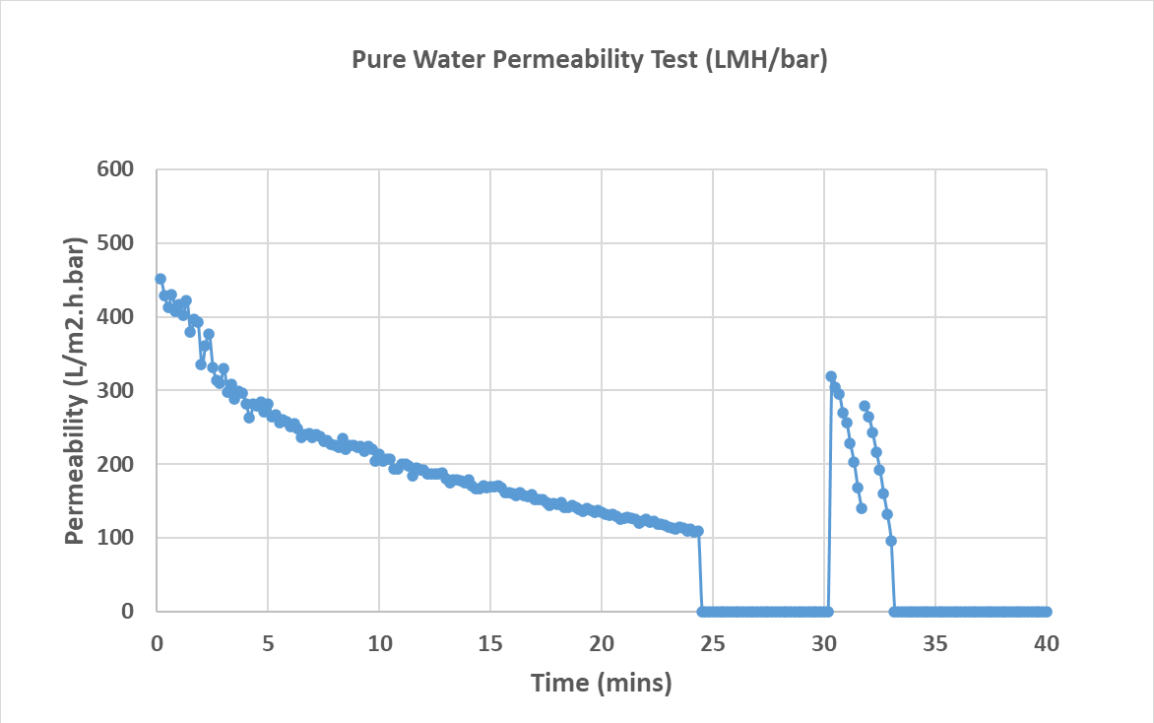

Figure 34 Membrane P filtering surface water without any pre-treatment with backwash pressure of 6 bar, duration of 5 minutes